UPCONVERSION NANOPARTICLE-BASED PHOTODYNAMIC INACTIVATION OF VIRUSES

LIM MENG EARN

B. Sc. (Hons.), University of Malaya

A THESIS SUBMITTED

FOR THE DEGREE OF MASTER OF ENGINEERING

DIVISION OF BIOENGINEERING

NATIONAL UNIVERSITY OF SINGAPORE

2011

Acknowledgements

I am extremely appreciative to my supervisors, Associate Professor Zhang Yong and Assistant Professor Justin Chu Jang Hann for their immense help and valuable guidance during the many hurdles I have encountered in my entire course of work. I am especially thankful to Mr. Shashi Ranjan and Ms. Niagara Muhammad Idris for their tremendous support and patience during the various scientific exchanges and discussions among us.

I would like to acknowledge Dr. Li Zhengquan and Dr. Amiya Priyam for their guidance in nanoparticle work as well as Ms. Chen Caiyun, Karen and Ms. Low Su Yin, June for mentoring me during my stint at the Department of Microbiology, Yong Loo Lin School of Medicine. I have learned many valuable virology research skills from them.

I thank all my labmates from Laboratory of Cellular and Molecular Bioengineering and Laboratory of Molecular RNA Virology and Antiviral Strategies who have helped me in some way or another. Furthermore, I would also like to thank Mr. Boh Boon Kim and Mr. Tan Kah Yap for their helpful sharings and encouragements.

Last but not least, I would like to give my heartfelt appreciations to my family members, especially my parents who stand beside me through thick and thin. Without their wholehearted love, all these would not be possible!

Lim Meng Earn

12 August 2011

List of Publications, Awards and Presentations

Publications

1. Lei Yin Ang*, Meng Earn Lim*, Li Ching Ong*, Yong Zhang. Applications of upconversion nanoparticles in imaging, detection and therapy. *Nanomedicine* 6(7): 1273-1288 (2011). *(* authors contributed equally)*

2. Meng Earn Lim, Yen-ling Lee, Yong Zhang, Justin Jang Hann Chu. Photodynamic inactivation of viruses using upconversion nanoparticles. *Biomaterials* 33(6): 1912-1920 (2012).

Award

1. Poster Presentation Award, 4th East Asian Pacific Student Workshop on Nano-Biomedical Engineering, Singapore, December 2010.

Presentation

1. Meng Earn Lim, Justin Jang Hann Chu, Yong Zhang. Development of nanoparticle-based photodynamic therapy as a novel anti-viral strategy. 4th East Asian Pacific Student Workshop on Nano-Biomedical Engineering, Singapore, December 2010. *(Poster Presentation)*

Summary

Current virus inactivation strategies are working toward targeted inhibition of viral replication machinery by antiviral drugs. In addition, vaccination is another widely used strategy. However, the genetic and serological heterogeneities of viruses hamper the development of effective vaccines or antiviral drugs that work against all viruses of different serotypes and strains. Meanwhile, viruses that mutate rapidly will render the vaccines or antiviral drugs to be ineffective.

An alternative strategy in virus inactivation can be achieved through a light-based approach called photodynamic therapy (PDT). This approach requires the excitation of light-sensitive materials called photosensitizers to produce reactive oxygen species which mediate the inactivation of viruses. PDT results in the direct inactivation of viruses without depending on the host-virus responses. Although photodynamic effect has been demonstrated against viruses, it has been slow in gaining acceptance, mainly because of the hydrophobicity of photosentizers and current light sources used, which have limited tissue penetration ability.

Here, we report a novel upconversion nanoparticle-based PDT to photodynamically inactivate viruses. In this strategy, photosensitizers are loaded onto the near-infrared (NIR)-to-visible upconversion nanoparticles (UCNs). When the nanoparticles are irradiated with NIR light at 980 nm, the UCNs emit visible light which is being absorbed by the photosensitizers. The excited photosensitizers then convert nearby molecular oxygen to toxic singlet oxygen species, which mediate viral inactivation. The UCNs act as nanocarriers of the highly hydrophobic photosensitizers as well as nanotransducers that convert NIR light to visible emissions necessary for the excitation of photosensitizers. The use of NIR light

introduces several advantages such as high light penetration depth *in vivo* and minimal photodamage to cells and tissues.

The synthesized UCNs emit strong upconversion fluorescence by producing visible emissions in the green and red regions with peaks at 545 nm and 658 nm respectively when the UCNs were being irradiated with NIR light at 980 nm. ZnPc was used as the photosensitizer in this work due to its high absorption coefficient and quantum yields. Singlet oxygen is consistently being released from the UCNs over time. Using both PEI-coated and mesoporous silica-coated UCNs, we observed a significant decrease in virus titers when the Dengue viruses were irradiated in the presence of UCNs, demonstrating the feasibility of UCN-based system for photodynamic inactivation of viruses. In another development, NIR light was shown to penetrate mouse tissues and photodynamic inactivation of viruses beneath the skin tissues was achieved.

The findings from this work demonstrate the feasibility of UCN-based PDT to photodynamically inactivate viruses with advantages over current PDT technique. Moreover, it further realizes the potential of utilizing this strategy in treating localized viral infections, especially thick lesions and warts of cutaneous diseases.

Table of Contents

List of Figures

List of Tables

List of Abbreviations

W	Watt
s	second
min	minute
h	hour
mL	milliliter
mV	millivolt
kJ/cm^2	kilojoule per centimeter square
DI water	Deionized water
DENV2	Dengue virus serotype 2
PEI-UCN	PEI-coated upconversion nanoparticle (without ZnPc)
ZnPc-PEI-UCN	ZnPc –loaded PEI-coated upconversion nanoparticle
ZnPc-MS-UCN	ZnPc –loaded mesoporous silica-coated upconversion nanoparticle

Chapter 1: Introduction

1.1 Overview to viruses

Virus is an infectious particle which replicates inside the host cells but remains metabolically inert outside the cells. The genetic material is made up of nucleic acids and may exist as deoxyribonucleic acids (DNA) or ribonucleic acids (RNA). These genes are protected by a protein coat called capsid. Some viruses have a lipid bilayer envelope with glycoproteins on the surface of the envelope. The viral envelopes play an important role in mediating the entry of viruses into the host organism. Viruses exist in various sizes and shapes which include helical, polyhedral, enveloped and binal.

Viruses transmit from one host organism to another via exchange of bodily fluid, airborne route, waterborne route or fecal-oral route. Upon entry into a host organism, such as human, a virus is activated and by intervening and utilizations of the host cells' metabolic machinery, the virus starts to replicate. During the virus replication cycle, the host cell undergoes cytopathic changes, which may activate the body's immune system or disrupt the body's physiology, eventually causing symptoms such as fever, flu, to swelling of blood vessels and gastrological disorder. In cases of severity, virus infection may lead to death when left untreated.

Infectious diseases caused by viruses are many and some of the serious diseases include acquired immune deficiency syndrome (AIDS), severe acute respiratory syndrome (SARS) and influenza. The spread of SARS and H1N1 swine flu pandemic recently was a public health emergency of international concern. Thus, despite their minuteness, viruses pose huge

life threats and economic lost which raise concerns of viruses as medically important pathogens in the 21st century.

1.2 Current virus inactivation strategies

Vaccination and antiviral drugs are currently the two clinically-adopted antiviral strategies. Although vaccination is capable of providing immunity when the person is still healthy, it is not effective against already-infected patients. In addition, viruses with high mutation rates such as influenza cause vaccines to be ineffective. There is also the possibility that the vaccines could harm the host by unintentional infection to the host. Due to its systemic immunity nature, vaccinations cannot be deployed to prevent virus infection at the localized level.

As for antiviral drugs which inactivate viruses based on targeted inhibition of virus replication machinery, the efficacy of the drugs is very much limited by genetic and serological heterogeneities of viruses. One example is the difficulty in developing an antiviral drug that is effective against all four serotypes of Dengue virus due to the differences between serotypes. Moreover, the toxicity and side effects of the antiviral drugs pose another major concern for the infected patients. Meanwhile, viruses that undergo high mutation rates like the influenza virus will render the newly developed drugs to be ineffective within few years. Along with vaccinations, antiviral drugs could not be used to treat localized virus infections as these drugs are normally applied systemically.

1.3 Photodynamic therapy (PDT): An alternative

PDT works via the excitation of light-sensitive materials called photosensitizers to produce reactive oxygen species (ROS) which mediate the inactivation of viruses. PDT inactivates viruses directly compared to vaccinations and antiviral drugs which depend on host-virus interactions. Hence, PDT offers an attractive alternative for the development of a potential antiviral strategy with therapeutical applications.

At present, the main therapeutic application for PDT is in the field of cancer [1, 2]. Although PDT is mainly applied for cancer therapy, it has been adopted to treat various non-oncological diseases as well. PDT has been reported to be effective against various bacterial, fungal and protozoan pathogens [3]. In fact, photodynamic processes in medicine was first demonstrated through the inactivation of a microorganism (*Paramecium caudatum*) from the lethal effect of acridine and visible light [4].

Although photodynamic effect has long been demonstrated against viral targets, the path leading to it being adopted clinically for treatment of viral diseases remains challenging with many hurdles [5]. Various problems with PDT such as impure photosensitizers, unspecific light sources and irregular dosimetry have slowed its adoption in mainstream medicine [6].

Common photosensitizers that have been employed to date in the photodynamic inactivation of viruses are dyes or its associated derivatives [7]. Usually, ultraviolet (UV) or visible light is used to excite the photosensitizers. However, these light sources have serious drawbacks, which include limited tissue penetration and dangerous carcinogenic and cytotoxic effects. In addition, cell pigmentation generally absorbs strongly in the visible light region . As most of the photosensitizers also absorb within this range, light energy delivered to the target site is

much reduced due to competitive absorption by the cell pigmentation. Moreover, the majority of photosensitizers aggregate easily in aqueous media due to their hydrophobicity. This results in altered chemical and biological properties.

1.4 Motivations and Objectives

Nanotechnology has contributed rapidly to the development of novel materials with excellent properties and functionalities. One particular example is the ultrafine particles called nanoparticles. Nanoparticles can be created from various materials and further fine tuned to deliver unique surface properties, leading to their rapid deployment in biomedicine. [8]. As photosensitizer carriers, nanoparticles show great promise in advancing the field of PDT and overcoming the associated limitations.

The objective of this project was to use upconversion nanoparticles for the development of upconversion nanoparticle-based photodynamic inactivation strategy. In order to achieve this objective, the following specific aims should be accomplished:

Synthesis of upconversion nanoparticles and ZnPc incorporation: Upconversion nanoparticles (UCNs) of sodium yttrium fluoride ($NaYF_4$) doped with ytterbium (Yb^{3+}) and erbium (Er^{3+}) were synthesized based on a hydrothermal method. Due to the surface properties, the synthesized nanoparticles were not soluble in water. To confer hydrophilicity, the nanoparticles were coated with a layer of polyethylenimine (PEI). PEI is a polymer with amino functional groups that renders nanoparticles hydrophilic. Zinc (II) phthalocyanine (ZnPc) photosensitizers were attached to the PEI coating via physical adsorption. In another design, the nanoparticles were first coated with a thin layer of silica followed by subsequent mesoporous silica coating which the ZnPc was later incorporated.

Photodynamic inactivation of viruses in suspension using the ZnPc-loaded nanoparticles: The UCNs were studied for their potential use in the development of UCN-based photodynamic inactivation system against viruses. For this purpose, Dengue virus serotype 2 (DENV2), an enveloped RNA virus, was used. To the best of our knowledge, the idea of nanoparticle-based photodynamic inactivation is novel and has not been reported elsewhere. The localized nature of PDT is best suited to treat viruses causing topical infections such as herpesvirus and papillomavirus. However, due to unavailability of the source, Dengue virus was used instead as an alternative model in this study. Hence, we wish to highlight here that it was never the objective of this study to develop the UCN-based photodynamic inactivation strategy for the treatment of Dengue virus infections such as Dengue hemorrhagic fever. The DENV2 merely acted as a virus model for this proof-of-concept study. Photodynamic inactivation of viruses in suspension was first carried out to assess the feasibility and efficacy of inactivating extracellular viruses using these nanoparticles. The photodynamic inactivation ability of the nanoparticles was studied with various parameters such as light fluence and nanoparticle concentration. Photodynamic inactivation of virus suspensions in the presence of mouse tissues was also performed to demonstrate the tissue penetration ability of near infrared (NIR) light.

1.5 Thesis overview

This thesis consists of 6 chapters and the organization of the thesis is as follows:

Chapter 1: Provides background information about current virus inactivation strategies and a closer look at PDT as an alternative.

Chapter 2: Presents the literature review of PDT and upconversion nanoparticles.

Chapter 3: Explores the use of PEI-coated UCNs for the photodynamic inactivation of viruses in suspension.

Chapter 4: Discusses the synthesis and characterizations of the mesoporous silica-coated UCNs.

Chapter 5: Presents the capability of mesoporous silica-coated UCNs to photodynamically inactivate viruses in suspension and the ability of NIR light to penetrate mouse tissues and inactivate viruses beneath the tissues.

Chapter 6: Summarizes the work done thus far of this project and provides key recommendations for future work.

Chapter 2: Literature Review

2.1 Photodynamic therapy (PDT)

PDT is an oxygen-dependent therapy which produces toxic reactive oxygen species (ROS) by light-activable photosensitizers. This oxygen-dependency distinguishes PDT from other types of photochemotherapy [9].

2.1.1 Mechanism of PDT

The mechanism of PDT can be divided into three stages, namely photosensitizer excitation, ROS production and cell death. Light emitting the suitable wavelength is employed to excite the photosensitizer. A particular light source is chosen such that its emission spectrum overlaps well with the absorption spectrum of the photosensitizer. When the photosensitizer absorbs light with appropriate wavelength, it is elevated electronically from ground state to excited state [10]. Excitation of the photosensitizers leads to either type I or type II reaction, resulting in ROS generation (Figure 2.1).

In type I reaction, the excited photosensitizers transfer their energy to a substrate, normally cell membrane or a molecule, which subsequently reacts with oxygen. On the other hand, the excited photosensitizers can also transfer their energy directly to the surrounding oxygen molecules (type II reaction). For type I reaction, the energy transfer between the photosensitizers and substrates generates reactive free radicals which react with oxygen and produces hydroxyl radicals, superoxide anion radicals and hydrogen peroxides [11]. Meanwhile, type II reaction which is commonly regarded as the dominant reaction produces singlet oxygen from the direct interaction with surrounding oxygen molecules [12].

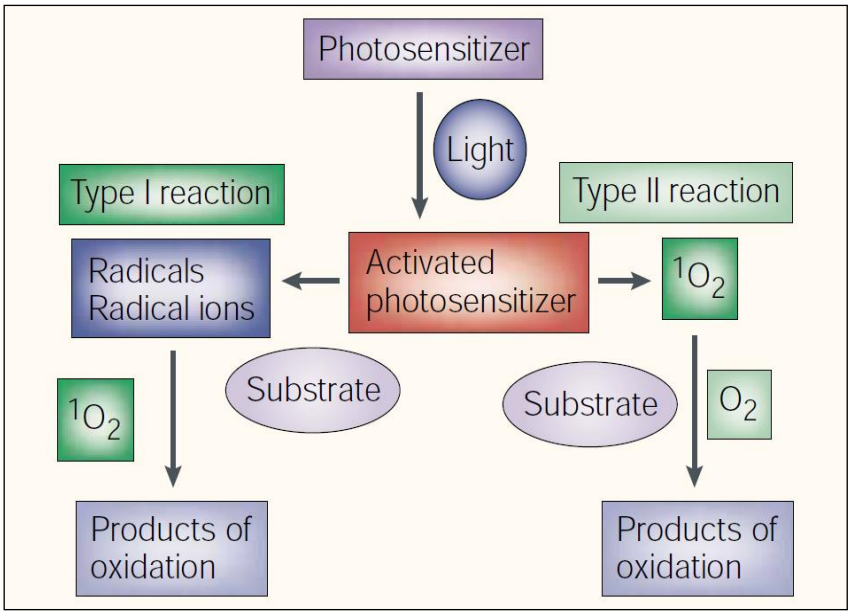

Figure 2.1 The light-excited photosensitizers can go through either type I or type II reaction, both of which eventually result in the production of ROS. (*Reproduced with permission from Nature Publishing Group)*

Singlet oxygen ($^1O_2$), can be produced through the interaction of ground state oxygen ($^3O_2$) with the excited photosensitizer molecule (P*):

$$P + \text{light} \rightarrow P^*$$

$$P^* + {}^3O_2 \rightarrow P + {}^1O_2$$

$^1O_2$ species has a very short lifetime (> 3.5 μs) and diffuses only 0.01 to 0.02 μm due to [13, 14]. As such, the damage causes by $^1O_2$ is bound to the immediate surroundings of the photosensitizers which have been exposed to light. This property of $^1O_2$ prevents it from interacting with distant targets, at the same time increasing its specificity [15]. Multiple regeneration of the $^1O_2$ species could occur due to the short lifespan of $^1O_2$, thus allowing consistent photodynamic actions within a short time period.

The formation of ROS such as $^1O_2$ or free radicals causes the oxidization of various cellular compartments such as mitochondria, plasma membrane and Golgi apparatus [16], resulting in

the destruction of the treated tissue. Damages to the cellular compartments lead to cell death mediated by apoptotic, necrotic or autophagic pathway [17]. Photosensitizers localized to the plasma membrane or lysosomes may sometimes block the apoptotic pathway, leading to induction of autophagy or necrosis [18]. Nevertheless, studies have suggested that apoptosis is the preferable outcome of PDT [16].

The above descriptions of the PDT mechanism are cell-based as the PDT of cancer is currently gaining clinical acceptance and its mechanism widely studied. However, PDT is also extended to the field of microbial infections and virus inactivation. The exact PDT mechanism to inactivate viruses is not fully understood. Type II reaction is widely recognized as the dominant reaction in causing photodynamic viral damage [7]. The extent of the PDT damage on viruses is depending on the chemistry of the photosensitizers used. Nucleic acid and viral envelope are the two target sites identified. Majority of the photosensitizers used in PDT against viruses, for example methylene blue and psoralens, are causing damage to the viral nucleic acid via an intercalative mechanism. Damage to the nucleic acids occurs through the oxidation of guanosine residues, leading to DNA or RNA damage [5]. Other photosensitizers such as phthalocyanines have been found to damage viral envelopes via reaction with phospholipids and peptides. The ROS interact with membrane lipids and stimulate lipid peroxidation while interaction with peptides are mainly through cycloaddition to tryptophan residues [19]. These reactions with viral envelope result in virus inactivation via conformational or structural degradation of the viruses [7].

2.1.2 State-of-the-art progress of PDT

A German medical student, Oscar Raab, was first to report in 1900 that the combination of light and acridine are cytotoxic to *Paramecium caudatum* [4]. The term "photodynamic action" was introduced by Von Tappeiner and Jesionek in 1903 based on their observations in the treatment of skin tumors by applying eosin to the tumor sites in conjunction with white light [20]. However, it was only until 1975 when Dougherty and his team reported the complete eradication of tumor in mice [21]. This development has led to the interest for PDT studies in cancer. Thus far, PDT treatment has been reported clinically on various cancerous tumors such as breast cancer tumors, gynecological tumors, head and neck tumors, colorectal cancer tumors, cutaneous malignancies, intraperitoneal tumors and pancreatic tumors [22-28]. Currently, PDT is recommended for patients with early-stage cancers because the cancers could not be operated on. However, in further studies, the effectiveness of PDT has been called into question due to issues with specificity and potency of photosenstizers.

2.2 Photodynamic inactivation of viruses by PDT

In 1928, Schultz *et al.* first reported the photodynamic inactivation of a virus, *Staphylococcus* bacteriophage using methylene blue [29] but it was only until the 1970s that the first PDT clinical trial in humans was first conducted to treat herpes genitalis, genital infection by herpes simplex virus [6]. However there were concerns that the neutral red photosensitizer converts healthy cells to malignant cells and causes damage to nucleic acids of surrounding healthy cells [30]. Subsequently trials were discontinued [31]. In view of all the problems, it seems that the use of photosensitizers for PDT treatment of topical vius infection is less appealing. Currently, herpes virus and papillomavirus are the two major viruses amenable to the photodynamic approach clinically. These two viruses have been the focus of PDT studies

on viruses due to their localized nature of infections. PDT has also been actively studied in the field of blood product disinfection, which greatly increased the range of susceptible viruses.

2.2.1 PDT of herpesvirus infection

The adoption of PDT to treat herpesvirus infection was first demonstrated on herpes genitalis and ophthalmic keratitis using neutral red and proflavine photosensitizers, they were shown to be effective [32, 33], however side effects were also seen [34]. The side effects for neutral red and proflavine photosensitizers have long been acknowledged. Nevertheless, risk of side effects increased using photosensitizers which are not pure with unoptimized dosimetry [35] coupled with the deployment of short-wavelength light sources [36]. In addition, the use of UV light necessary to excite proflavine contributed more damages to the host. Compared to the control (without treatment), UV light's mutation rate was shown to be 15 to 20 times higher [37].

2.2.2 PDT of papillomavirus infection

HPD and dihematoporphyrin ether (HPE) were used as the photosensitizers for PDT of laryngeal papillomata, an infection caused by human papillomavirus (HPV) [38, 39]. The results of this treatment were not encouraging and photosensitization of the skin after treatment was regularly seen [40].

In 1999, 5-aminolevulic acid (ALA) received clearance from the Food and Drug Administration (FDA) as a medication for localized PDT therapy of nonhypertrophic actinic keratoses [41]. ALA is a photosensitizing agent which could penetrate into underlying tissues

where it is being converted into protoporphyrin IX (PpIX) photosensitizer. This ALA-PDT was reported to be effective against human immunodeficiency virus (HIV) and herpesvirus *in vitro* and *in vivo* [42]. In addition, this localized ALA-PDT treatment has also been adopted to treat warts such as *Verrucae vulgaris* and *Molluscum contagiosum* [43] which are caused by papillomavirus and Molluscum contagiosum virus (a human pox virus) respectively. However, this therapy yields phototoxic reaction such as pain, stinging, itching, burning and hyperpigmentation (Figure 2.2).

Figure 2.2 Phototoxic reaction of ALA-PDT resulting in patients experiencing pain, stinging, burning, itching and hyperpigmentation. *(Reproduced with permission from Elsevier Limited)*

2.2.3 PDT in blood disinfection

Donated whole blood may be used in direct replacement for blood loss in trauma or surgery, or it may be separated physically into a number of useful blood products. To achieve sufficient levels of these factors, plasma fractions are concentrated or pooled together. Blood plays an important role in transporting oxygen and nutrients around the human body. However, it can also carry pathogens, especially in the blood of an infected person. The most common example is the presence of HIV in the blood due to blood-to-body fluid contact with

an infected person or syringe. Contaminating pathogens in blood cover a huge range, depending on the history of the donor and the degree of care taken in the handling of the donation in the processing stage.

Inactivation of viruses in blood can be complicated because blood is a heterogeneous mix of various components. Intracellular pathogens which reside in blood cells are especially protected against physical methods such as filtration or washing. Detergent has been successfully used for virus inactivation in plasma but they are unsuitable for platelets and erythrocytes as they can damage the cellular membranes [44].

The use of PDT in blood disinfection can reduce collateral damage. Three procedures are used clinically or approved for clinical trials: methylene blue (with visible light) [45], amotosalen HCl (with UV light) [46] and riboflavin (with UV light) [47]. Of these three, the methylene blue-mediated is a more established means of blood product disinfection. The amotosalen HCl and riboflavin procedures employing UV light potentially lead to host damage due to high mutation frequency. In the methylene blue procedure, the plasma is filtered through a membrane to eliminate cellular contamination The plasma is subsequently mixed with methylene blue hydrochloride and illuminated at 590nm for 20 minutes. Residual methylene blue and its photo-products are later removed through filtration. [48]. Although this method is effective in significantly reducing viral count, it also decreases fibrinogen activity, which is important for blood coagulation. Due to such safety concerns, extensive studies have been done to determine the safety of PDT in its clinical applications such as virus inactivation in blood [49].

2.3 Factors that affect the efficacy of current PDT technique

2.3.1 Photosensitizer hydrophobicity

Photosensitizer hydrophobicity is important in determining antiviral activity. Majority of photosensitizers are highly hydrophobic and normally aggregate in aqueous solutions, affecting their photochemical and photobiological properties. In addition, first generation photosensitizers possess limitations such as low specificity and high collateral damage. Considerable efforts have been made to overcome this by means of drug delivery system [50].

2.3.2 Light source

Current light sources which are in the UV or visible light region have limited tissue penetration ability which restricted the amount of light to be delivered to the target sites and thus reduced PDT efficacy in treating localized infected tissues. In addition, cell pigmentation usually absorbs strongly in the visible light region which overlaps well with the absorption spectra of most photosensitizers and better light sources are needed in order to avoid weakening light delivery to the target site due to competitive absorption of cell pigmentation.

2.4 Upconversion nanoparticles (UCNs)

2.4.1 Upconversion mechanism

The exact mechanisms involved in upconversion are varied and complex and can be found to operate in isolation or in combination [51]. Upconversion is a non-linear optical process involving multiple stages of absorption and fluorescence which results in generation of shorter wavelengths. Excitation and emission entities (usually ions) are involved in producing upconversion phenomenon (Figure 2.3). When excited with energy of suitable wavelength, both excitation and emission entities achieve a higher excitation state. However, instead of radiative dissipation, the excitation entity non-radiatively transmits the excess energy to emission entity, thereby pushing it to a still higher excited state. The emission entity subsequently returns to the ground state and excess energy is emitted as short wavelengths of high energy.

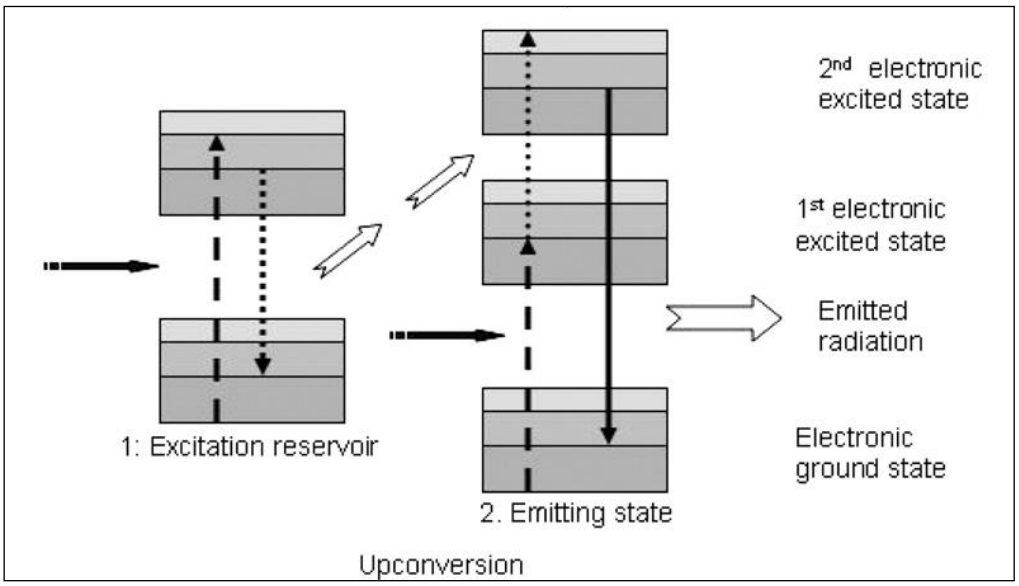

Figure 2.3 Mechanism of upconversion process. *(Reproduced with permission from Elsevier Limited)*

2.4.2 UCN core materials and dopants

The basic structure of UCNs consists of transition metal (3d, 4d, 5d), lanthanide (4f), or actinide (5f) dopant ions embedded in the lattice of an inorganic crystalline host. Of these dopant ions, the trivalent lanthanides are predominantly used because most of them (except La^{3+}, Ce^{3+}, Yb^{3+}, and Lu^{3+}) have multiple metastable states, making them well-suited for UC. Although a single lanthanide ion is sufficient to produce the upconversion effect, co-doping is usually favored as most lanthanide ions have low absorption cross-sections leading to weak emission. To enhance upconversion efficiency, co-doping between two different lanthanide ions, the first serving as absorber and other acts as emitter, is generally done. Ytterbium (Yb^{3+}) ion, which possesses larger absorption cross-section in the NIR region, is often used as the absorber ion. Erbium (Er^{3+}), thulium (Tm^{3+}) and holmium (Ho^{3+}) ions, on the other hand, are frequently used emitter ions due to their equally spaced energy levels that facilitate photon absorption and energy transfer in upconversion processes [52].

Another important component of UCNs is the host materials, which determines the optical properties and emission efficiency. The desired host materials should have close lattice matches with the dopant ions and low lattice phonon energies to minimize energy losses and maximize radiative emissions. Halide-based compounds are mostly used due to their low phonon energies but the hygroscopic nature of the heavier halides makes the fluorides a more popular choice [52]. To date, many host materials as well as lanthanide dopant ions have been utilized to synthesize UCNs with different emissions by varying host-dopant combinations [52]. Among these lanthanide-doped UCNs, $NaYF_4$ co-doped with Yb^{3+}/Er^{3+} and Yb^{3+}/Tm^{3+} nanoparticles have been reported as the materials which produce superior upconversion capabilities [53].

2.4.3 UCN-based PDT

UCNs with its unique optical properties, provide a possible solution to all the limitations faced by the current PDT technique. First of all, the ability of these nanoparticles to convert NIR radiation to visible light can expand the use of PDT due to the greater light penetration of NIR in biological tissues [54]. Moreover, cells and tissues absorb weakly in the optical window of the NIR region. Thus, the use of NIR light resolves the issue of weakening light delivery due to absorption of light by cell pigmentations or hemoglobin in blood. Although not many literatures can be found on the use of UCNs for PDT, the development of UCN-based PDT as a novel treatment modality has attracted considerable interests recently. Current works on UCN-based PDT are focusing on its use for cancer treatment and can be classified into polymer-based and silica-based approaches.

In the polymer-based approach, PEI and PEG have been used to provide capping layers in which photosensitizers get ensconced. Our group [55] attached zinc phthalocyanine (ZnPC) photosensitizers to the surface of PEI-coated UCNs by physical adsorption. Folic acid was further conjugated for specific targeting to the colon cancer cells. Results showed reduced cell viability upon NIR irradiation. Ungun *et al.* [56] has synthesized three-layer nanoparticles consisting of $NaYF_4$: Yb^{3+}, Er^{3+} UCNs as the core, porphyrin photosensitizers as the middle layer and a PEG polymer coat as the outer layer. They have demonstrated high photosensitizer-to-UCN ratio of 1:3 but the PDT efficacy of these UCNs has not been proven. The other design utilizes silica as a protective layer in which the photosensitizers are impregnated. Using such a strategy, Zhang *et al.* [57] doped merocyanine-540 photosensitizers into silica-coated UCNs which were further functionalized with breast cancer-targeting antibodies. Based on the optical and fluorescence images obtained, UCN-treated cancer cells were dead or gradually dying after NIR irradiation. In this case, the

release of ROS is hampered by the non-porous silica, therefore resulting in low PDT efficacy. By using mesoporous-silica-coated UCNs, release of ROS and oxygen diffusion will not be hampered. Our group [58] reported such mesoporous UCNs in which the particles were first coated with a thin layer of silica followed by subsequent coating of mesoporous silica layer which was loaded with ZnPc. Cell viability of the treated bladder cancer cells was significantly lower compared to the controls. Additionally, production of singlet oxygen from these ZnPc-loaded nanoparticles in live cells has been proven [59].

Although UCN-based PDT has been shown to be a potential therapeutic option against cancer cells, no attempt is made to explore the possibility of inactivating viruses via this UCN-based approach which could potentially be a novel antiviral strategy.

Chapter 3: PEI-coated UCNs for photodynamic inactivation of viruses

3.1 Introduction

Although photodynamic inactivation of viruses via PDT has been reported, acceptance of this therapy is considerably low due to several shortcomings such as light sources with limited tissue penetration ability, hydrophobic photosensitizers and skin photosensitivity for prolonged periods. Nanoparticles, in this case, upconversion nanoparticles (UCNs), are used in the development of 'nano-transducers' that could potentially address the shortcomings of the current PDT set-up.

In our group, we have synthesized UCNs that consist of $NaYF_4$ nanocrystals co-doped with the lanthanide ions Yb^{3+} and Er^{3+} surrounded by a layer of PEI. ZnPc, the photosensitizer, is physically adsorbed to the surface of PEI-coated UCNs [60] (Figure 3.1).

Upon NIR irradiation at 980 nm, both Yb^{3+} and Er^{3+} ions are excited to metastable excited state. Yb^{3+} ion, which normally acts as absorber ion due to its large absorption cross-section in the NIR region, will then return to ground state and transfers its energy non-radiatively to Er^{3+} ion. Er^{3+} ion then attains higher excited state and correspondingly emitting a high energy photon when it recedes to the ground state. The PEI-coated $NaYF_4$:Yb^{3+}/Er^{3+} UCNs convert NIR light to visible light with two distinct peaks at 510-570 nm (green) and 640-680 nm (red) regions. ZnPc absorbs the fluorescence emitted by the doped ions and becomes excited to a triplet state. This triplet state is not long-lived and when it returns to the original ground-state, the energy released by ZnPc diffuses to the surrounding. Nearby molecular oxygen are converted to singlet oxygen species, which would result in viral inactivation through genome

(DNA or RNA) destruction, probably through oxidative degradation of guanine residues or structural degradation of the virus itself (as discussed in Section 2.1.1).

The PEI-coated UCNs were synthesized with established protocol (one-pot synthesis using a hydrothermal method) and well-characterized by our group members [60]. As mentioned in Section 2.4.2, $NaYF_4$ was chosen as the host material due to its superior upconversion capability when co-doped with Yb^{3+} and Er^{3+}.

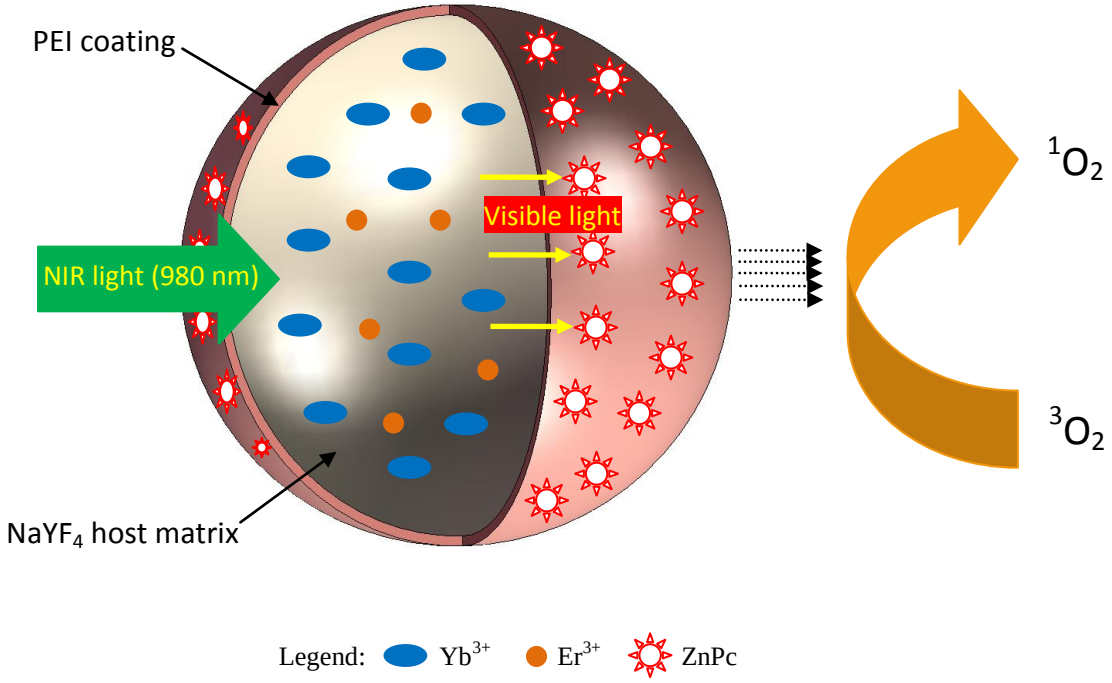

Figure 3.1 Schematic drawing of structure and mechanism of action of the PEI-coated ZnPc-attached UCN.

PEI is a hydrophilic polymer consisting of a number of amino groups. The advantages of incorporating PEI coating are that it solubilizes the non-polar $NaYF_4$:Yb^{3+}/Er^{3+} nanocrystallie core in aqueous solutions and confers functional groups for bioconjugation. Both low molecular weight and high molecular weight PEI have been used to synthesize the nanoparticles. However, uniform nanoparticles with regular size and shape were obtained

with the use of high molecular weight PEI as it contains more coordination sites which facilitate enhanced binding of PEI to the UCN surface and reduce nanoparticles aggregation efficiently.

The synthesized particles are 50 nm in diameter (by average), spherical and monodispersed. High crystallinity of the nanoparticles was observed with hexagonal phase as the dominant phase and a secondary cubic phase. Upon excitation by 980 nm NIR light, the nanoparticles emit visible lights with dual peaks in the green and red regions at 540 nm and 655 nm respectively in aqueous solutions. The combination of these two peaks yielded the resultant visible emission which appears greenish-yellow.

ZnPc is bound to the surface of the nanoparticles via physical adsorption. Phthalocyanine is a non-polar macrocyclic compound which bears structural similarity to porphyrin, except at the tetrapyrrolic rings. The presence of the central metal ion, in this case zinc ion, stabilizes the structure and gives high yield of singlet oxygen (Figure 3.2). ZnPc was chosen because it is the second generation photosensitzer with desired properties such as high absorption coefficient (2.5×10^5 M^{-1}/cm), effective singlet oxygen generator and rapid removal from the body [61, 62]. Moreover, the excitation of ZnPc falls within the red region with excitation maximum at 674 nm which overlaps considerably with the red emission of the PEI-coated UCNs in the range of 650-675 nm. The overlapping allows ZnPc, in close contact with the nanoparticles, to absorb the visible emissions released by the nanoparticles after being exposed to NIR irradiation at 980 nm.

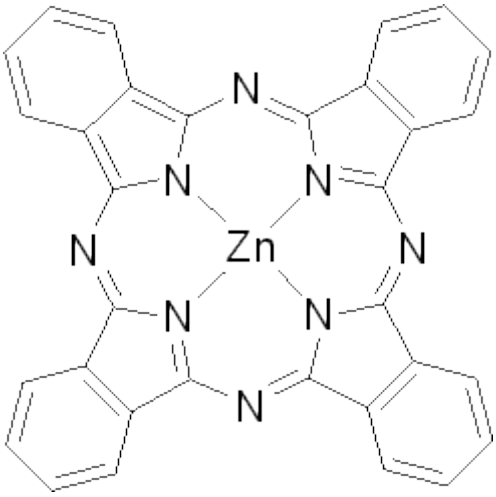

Figure 3.2 Chemical structure of ZnPc photosensitizer *(from Sigma-Aldrich's website; http://www.sigmaaldrich.com/catalog/product/aldrich/341169?lang=en&region=SG)*

These PEI-coated UCNs have been well-characterized and used in our group for PDT in cancer cells [55]. In this chapter, the feasibility of the UCN-based photodynamic inactivation system was explored by using these well-characterized UCNs.

3.2 Materials and Methods

3.2.1 Materials

Polyethylenimine (PEI, branched polymer (-$NHCH_2CH_2$-)x(-$N(CH_2CH_2NH_2)CH_2CH_2$-)y) of molecular weight 25kD, sodium chloride (NaCl, ≥ 99.0%), yttrium chloride hexahydrate (YCl_3•$6H_2O$, 99.99%), ytterbium oxide (Yb_2O_3, 99.99%), erbium oxide (Er_2O_3, 99.99+%), ammonium fluoride (NH_4F, 98+%), zinc phthalocyanine (ZnPc, 97%), Roswell Park Memorial Institute-1640 (RPMI-1640) medium, L-15 medium (Leibovitz), crystal violet, methanol, bovine serum albumin (BSA) were purchased from Sigma-Aldrich, USA. Fetal bovine serum (FBS) and penicillin-streptomycin were purchased from PAA Laboratories GmbH, Austria. Trypsin-EDTA and (0.5% Trypsin with EDTA•4Na) was purchased from GIBCO Invitrogen, USA. Phosphate-buffered saline (PBS) was purchased from 1st Base, Singapore. Sodium bicarbonate and formaldehyde (37%) were purchased from Merck KGaA, Germany. Carboxymethylcellulose (CMC) sodium salt (Aquacide II) was purchased from EMD Chemicals, USA. VD-IIIA diode pumped solid-state (DPSS) NIR Laser Driver was purchased from PhotoniTech, Singapore.

3.2.2 Synthesis of PEI-coated $NaYF_4$:Yb^{3+}/Er^{3+} nanoparticles

PEI-coated $NaYF_4$:Yb^{3+}/Er^{3+} nanoparticles were synthesized using a hydrothermal synthetic procedure developed in our laboratory [60]. 10 mL NaCl, 8 mL YCl_3, 1.8 mL $YbCl_3$, 0.2 mL $ErCl_3$ and 20mL PEI (25 kDa) were added to 60 mL ethanol. A suitable amount of NH_4F was later added after gentle stirring. The solution was then transferred to a Teflon-lined autoclave flask and heated at 200 ^oC for 24 h with continuous stirring. Nanoparticles were collected by centrifugation followed by a few times of washing with ethanol and DI water. Subsequently,

the nanoparticles were vacuum-dried and kept in DI water at room temperature. ZnPc was attached to the nanoparticles' surface via physical adsorption by adding the same volumes of ZnPc (500 nM) and nanoparticles (4.4 mg/mL) in ethanol before shaking gently for 30 minutes in room temperature. The mixture was centrifuged at 10000 rpm for 10 min, supernatant was cautiously withdrawn and the particles were resuspended in PBS. The nanoparticles were washed twice to remove unbound ZnPc.

3.2.3 Cell culture

Two cell lines were cultured and used for different experiments. The cell lines were BHK-21 (baby hamster kidney cells) and C6/36 (*Aedes albopictus* mosquito cells). BHK-21 cells were cultured in RPMI-1640 medium while C6/36 cells were cultured in L15 medium. All the cell culture media were supplied with FBS and penicillin-streptomycin as antibiotics. For L15 medium, FBS was heat inactivated at 56 ^{o}C for 30 min before being added into the medium. Cell culture media that were supplemented with 10% FBS were used as growth media for the cell lines while cell culture media with 2% FBS were used as maintenance media to enable cell survival. The pH of RPMI-1640 was adjusted to the range of 7.2 – 7.4 with sodium bicarbonate. All the cells, except C6/36 cells, were cultured in 75 cm^2 flasks and incubated in a humidified incubator with 5 % CO_2 at 37 ^{o}C. C6/36 cells were incubated in dry incubator without CO_2 at 28 ^{o}C.

Cells were sub-cultured from confluent monolayer. The cell culture medium was first discarded and the cell monolayer was washed with 5 mL of PBS. 2 mL of trypsin was then added and the flask was placed in an incubator for 3-5 min at 37 ^{o}C to detach the cells from the flask. 8 mL of cell culture medium was added to the cell suspension to neutralize the

enzymatic activity of trypsin. Multiple pipetting of the cell culture medium resulted in a single cell suspension. An appropriate amount of cells was re-seeded in the flask and the rest of the cells were discarded. The flask was then incubated in an incubator at an appropriate temperature. Cell monolayer that reaches confluency in 3 to 4 days was used for experiments.

To seed a certain amount of cells for experiments, cell counting using hemocytometer was used. The hemocytometer and glass coverslip were first cleaned with 70% ethanol. The coverslip was placed over the hemocytometer surface at a height of 0.1 mm so that the total volume for each of the nine 1 mm^2 squares of the counting grid is 0.1 mm^3. After trypsinization, one drop of cell suspension was introduced into one of the V-shaped wells with a micropipetter and the area under the coverslip was filled by cell suspension due to capillary action. The hemocytometer was then placed on a microscope stage and the counting grid was observed under 10X objective using a brightfield microscope. The cells in the four corner squares were counted. Only the cells on the top and left-hand sides of each square were included to avoid bias. The average number of cells in each square was used to calculate the cell concentration:

$$\text{Cell concentration (cells/mL)} = \text{Average number of cells per square} \times 10^4$$

3.2.4 Infection of cells

3.2.4.1 Viruses used

The virus used was Dengue virus serotype 2 (DENV2, New Guinea C strain) which was propagated on C6/36 cells. Viruses were harvested at the appropriate timing post-infection (p.i.) from the virus-infected cells.

3.2.4.2 Preparation of virus stock

The cell culture medium was discarded and the cell monolayer was rinsed with 5 mL of PBS. Multiplicity of Infection (M.O.I.) of 10 was used. 1 mL of virus suspension was used for the infection of cell monolayer in a 75cm^2 flask. The flask was incubated at 37 ^{o}C for 1 hour and rocked every 15 minutes to ensure even infection of the whole flask. After 1 hour, 14 mL of maintenance medium (cell culture medium with 2 % FBS) was added to the flask. The cells were incubated at 28 ^{o}C until the cytopathic effects of the respective cell lines became pronounced. DENV2 was harvested after four days of incubation, when syncytial formation on C6/36 cells was completed. To harvest the viruses, the extracellular virus-containing supernatants were collected and spun at 1500 rpm for 10 minutes to remove cellular debris. The virus supernatants were then aliquoted into sterile cryovials, sealed and immediately stored at -80 ^{o}C.

3.2.4.3 Plaque Assay

The amount of viruses harvested was determined and the virus titer, which is the concentration of infectious viral particles, was calculated. Ten-fold serial dilutions of the DENV2 samples up to the dilution factor of 10^{-6} were prepared in maintenance media of RPMI 2 % FBS. Aliquots of 100 µL from the appropriate dilutions were inoculated in triplicates onto monolayers of confluent BHK-21 cells grown in sterile 24-well tissue culture plate (plated at 62,500 cells/well). The virus-inoculated monolayers were incubated for an hour at 37 ^{o}C with rocking every 15 min to ensure even distribution of virus inocula. After 1 h of incubation, the inocula were removed upon washing thrice with PBS. 1 mL of semi-solid medium, 2 % carboxymethylcellulose (CMC) in cell culture medium containing 2 % FBS, was then layered onto the virus-infected cell monolayers. The plates were incubated at 37 ^{o}C in a humidified incubator with 5 % carbon dioxide for five days. After incubation, circular zones of infected cells called plaques were formed. Plaques were visualized by staining the cell monolayer with 0.5 % crystal violet solution overnight at room temperature. Plaques were counted and only wells in the range of between 10 and 100 plaques were accounted for in order to minimize error. Number of plaques counted, in combination with the dilution factor from which the plaques were counted were used to calculate the virus titer, expressed as plaque-forming units per millilitre (PFU/mL). PFU values indicate the number of infectious virus particles for a particular sample with an assumption that a single plaque represents an infectious virus particle.

3.2.5 Photodynamic inactivation of viruses in suspension

We first performed an experiment to examine the feasibility of this novel strategy by irradiating 100 µl of DENV2 (6.36 $\log_{10}$ PFU/mL) in L15 medium each containing 0.5 mg/mL ZnPc-attached PEI-coated UCNs (ZnPc-PEI-UCNs), 0.5 mg/mL PEI-UCNs (without ZnPc) and 0.1 mM ZnPc . A control sample containing only DENV2 suspension was also incorporated for this study. All these samples were exposed to NIR irradiation (980 nm) at the fluences of 20 and 40 kJ/cm^2 (laser power of 0.47 W and irradiation time of 14 min 11 s and 28 min 22 s respectively). Additionally, a similar set of samples which act as dark controls were prepared in parallel and kept in the dark without NIR irradiation for the same period of time as the irradiation time of the samples exposed to NIR light. All the viral samples were then collected and virus titers of DENV2 were determined by plaque assay using BHK-21 cell line based on the method mentioned in Section 3.2.4.3. Reduction in virus titers was obtained by subtracting the virus titers of the NIR light-treated samples from the virus titers of their associated dark controls. Photodynamic inactivation efficacy was assessed based on percentage reduction of virus titer. Percentage reduction of virus titer was calculated based on the formula given below:

$$\text{Percentage reduction of virus titer (\%)} = \frac{\text{Virus titer of dark control sample (Light -)} - \text{Virus titer of light-treated sample (Light +)}}{\text{Virus titer of dark control sample (Light -)}} \times 100\ \%$$

The percentage reduction of virus titer tells us the reduction of infectious virus particles due to photodynamic treatment. Hence, greater photodynamic inactivation efficacy is achieved with higher percentage reduction of virus titer.

Fluence which describes the energy delivered per unit area, is a term normally used for light dosimetry with J/cm^2 as its unit:

$$\text{Fluence } (J/cm^2) = \frac{\text{Light source power (W) x Irradiation time (s)}}{\text{Laser beam area } (cm^2)}$$

Since the same light source was used throughout the project, laser beam area remained constant. According to the vendor of NIR laser driver (PhotoniTech, Singapore), the laser beam was in square shape with 0.2 cm in length and 0.1 cm in width. Thus, the laser beam area was calculated as 0.02 cm^2 (0.2 x 0.1 cm^2).

In another study to investigate the effect of nanoparticle concentration on the photodynamic inactivation efficacy, 100 µL of DENV2 (6.36 $\log_{10}$ PFU/mL) in L15 medium (DENV2 virus suspension) were mixed with a range of ZnPc-PEI-UCN concentrations (0, 2, 4.4, 44, 440, 4400 µg/mL) in 96-well tissue culture plate under aseptic conditions. These samples were irradiated with NIR light at 980 nm using VD-IIIA DPSS NIR Laser Driver at the fluence of 14 kJ/cm^2 (0.47 W and irradiation time of 10 min) with the distance between the light source and the viral samples at 5 cm. A similar set of samples were also prepared and they were kept in the dark for the same duration as the NIR irradiation time of the light-treated samples. The treated samples were then stored in cryovials at -80 ^oC and virus titers were determined via plaque assay as described in Sections 3.2.4.3. All experiments were performed in triplicate. Reduction in virus titers was obtained by subtracting the virus titers of the NIR light-treated samples from the virus titers of their associated dark controls. Photodynamic inactivation efficacy was assessed based on percentage reduction of virus titer as described in the feasibility study above.

3.3 Results and Discussion

3.3.1 Physical properties of PEI-coated $NaYF_4:Yb^{3+}/Er^{3+}$ nanoparticles

In order to investigate the feasibility of UCN-based photodynamic inactivation system as a novel anti-viral strategy, the design of PEI-coated $NaYF_4:Yb^{3+}/Er^{3+}$ nanoparticles was first employed as the pilot model for this purpose. Transmission electron microscopy (TEM) images showed that the nanoparticles were spherical with a mean particle size of 50 nm in diameter [60].

Upon exposure to NIR irradiation at 980 nm, the nanoparticles exhibit fairly strong upconversion fluorescence by producing green and red emissions with peaks at 540 and 655 nm respectively. Characterization studies demonstrated that the UCN emissions remain stable in various conditions and are biocompatible *in vitro*. The fluorescence spectrum of the nanoparticles and the findings of various characterization studies including the determination of singlet oxygen production via disodium 9,10-anthracenedipropionic acid (ADPA) assay and cell viability via MTT assay as well as their usage for PDT in cancer cells have been published by our group members [55, 60].

3.3.2 Feasibility of UCN-based system for photodynamic inactivation of viruses

As this UCN-based system has not been studied elsewhere, photodynamic inactivation of DENV2 in suspension was first carried out to explore the effectiveness of these nanoparticles.

Based on the results obtained, the virus titers reduced significantly ($P < 0.05$) when DENV2 virus suspension was mixed with 0.5 mg/mL ZnPc-PEI-UCNs and irradiated at both the fluences of 20 and 40 kJ/cm^2 (Figure 3.3 – Figure 3.6). When DENV2 virus suspensions was irradiated at the fluence of 20 and 40 kJ/cm^2 in the presence of 0.5 mg/mL ZnPc-UCNs, the virus titers were reduced from 7.26 $\log_{10}$ PFU/mL to 3.49 $\log_{10}$ PFU/mL (a 3.77 $\log_{10}$ PFU/mL or 52 % reduction) and from 7.16 $\log_{10}$ PFU/mL to 2.94 $\log_{10}$ PFU/mL (a 4.22 $\log_{10}$ PFU/mL or 58 % reduction) in infectious virus titer respectively. This suggested that more than 50 % of the viruses were photodynamically inactivated by ZnPc-UCNs. Meanwhile, a minor reduction of infectious virus titers as compared to their respective dark controls were observed for the DENV2 virus suspensions added with 0.5 mg/mL PEI-UCNs and 0.1 mM ZnPc and irradiated at both the fluences of 20 and 40 kJ/cm^2. Although capable of producing visible emissions for photosensitizer excitation, the PEI-UCNs do not carry ZnPc photosensitizers necessary to effect photodynamic inactivation. On the other hand, photodynamic inactivation effect was also not seen on virus suspension mixed with ZnPc as the NIR light at 980 nm is beyond the absorption range of this photosensitizer.

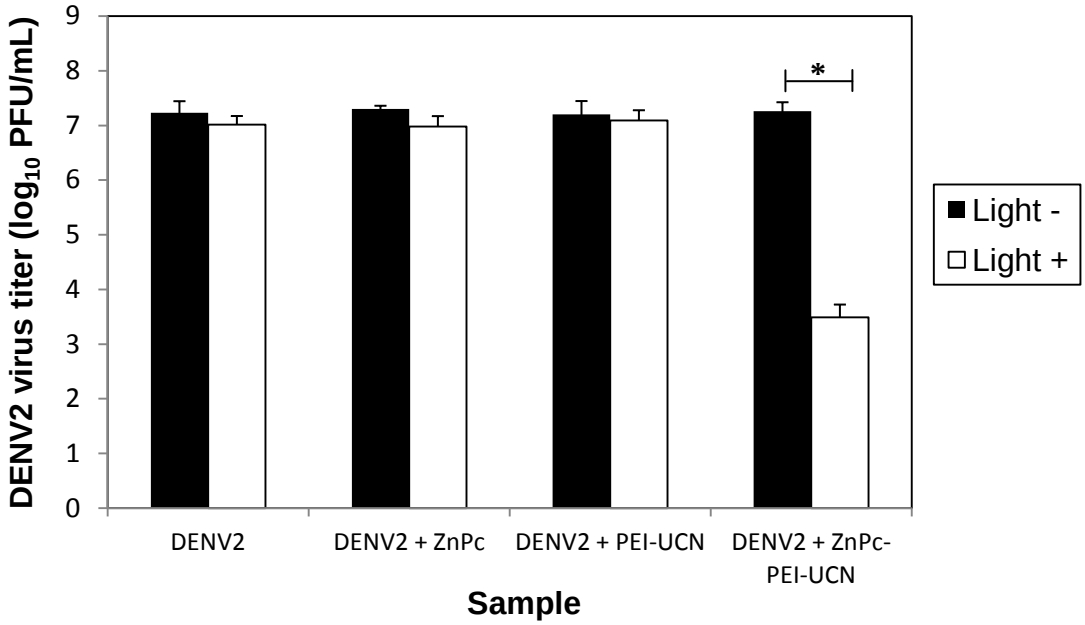

Figure 3.3 Infectious virus titers of DENV2 irradiated at the fluence of 20 kJ/cm^2 in the presence of 0.1 mM ZnPc photosensitizers, 0.5 mg/mL PEI-UCNs and 0.5 mg/mL ZnPc-PEI-UCNs. All experiments were performed in triplicate and error bars represent standard deviations of the mean. Statistical analysis was done by comparing light-treated samples to their respective dark controls using Student's t-test, ***** $P < 0.05$.

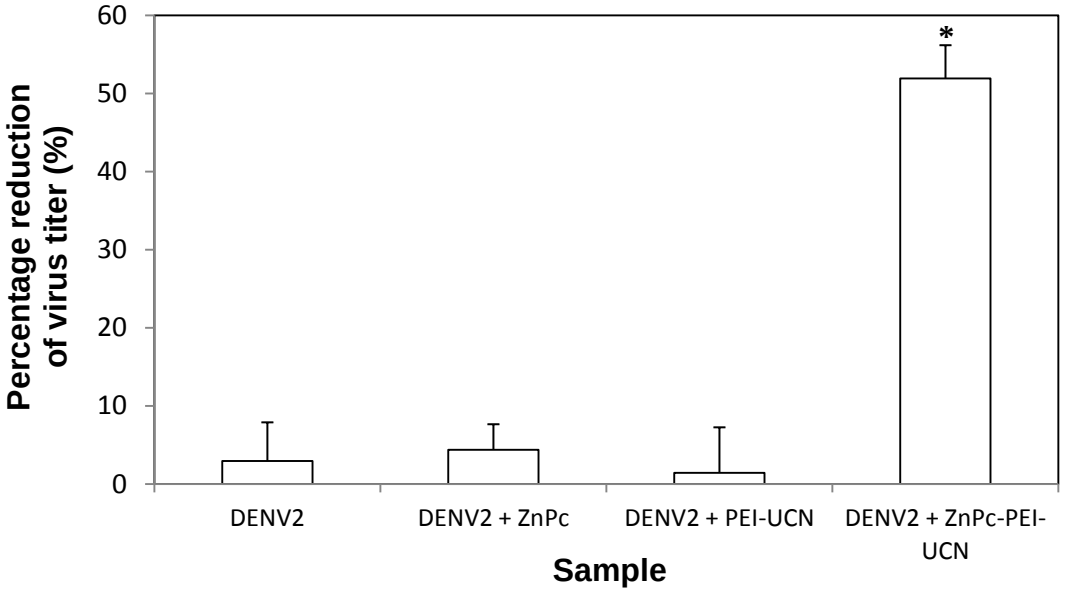

Figure 3.4 Percentage reduction of virus titer for DENV2 irradiated at the fluence of 20 kJ/cm^2 in the presence of 0.1 mM ZnPc photosensitizers, 0.5 mg/mL PEI-UCNs and 0.5 mg/mL ZnPc-PEI-UCNs. Error bars represent standard deviations of the mean. Statistical analysis was done by comparing the samples to the control (the DENV2-only sample) using Student's t-test, ***** $P < 0.05$.

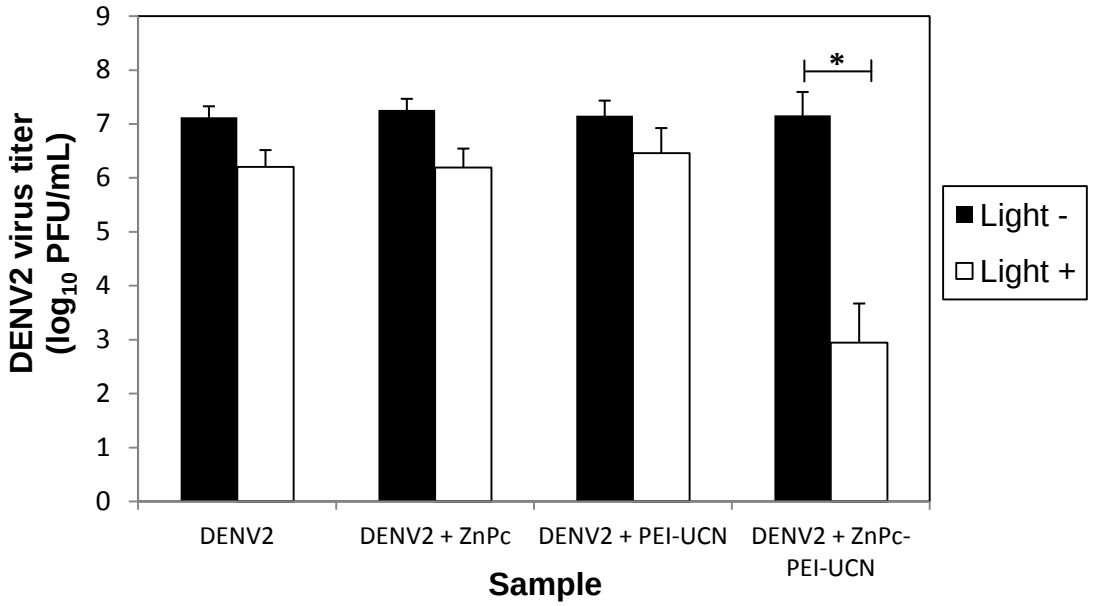

Figure 3.5 Infectious virus titers of DENV2 irradiated at the fluence of 40 kJ/cm^2 in the presence of 0.1 mM ZnPc photosensitizers, 0.5 mg/mL PEI-UCNs and 0.5 mg/mL ZnPc-PEI-UCNs. All experiments were performed in triplicate and error bars represent standard deviations of the mean. Statistical analysis was done by comparing light-treated samples to their respective dark controls using Student's t-test, ***** $P < 0.05$.

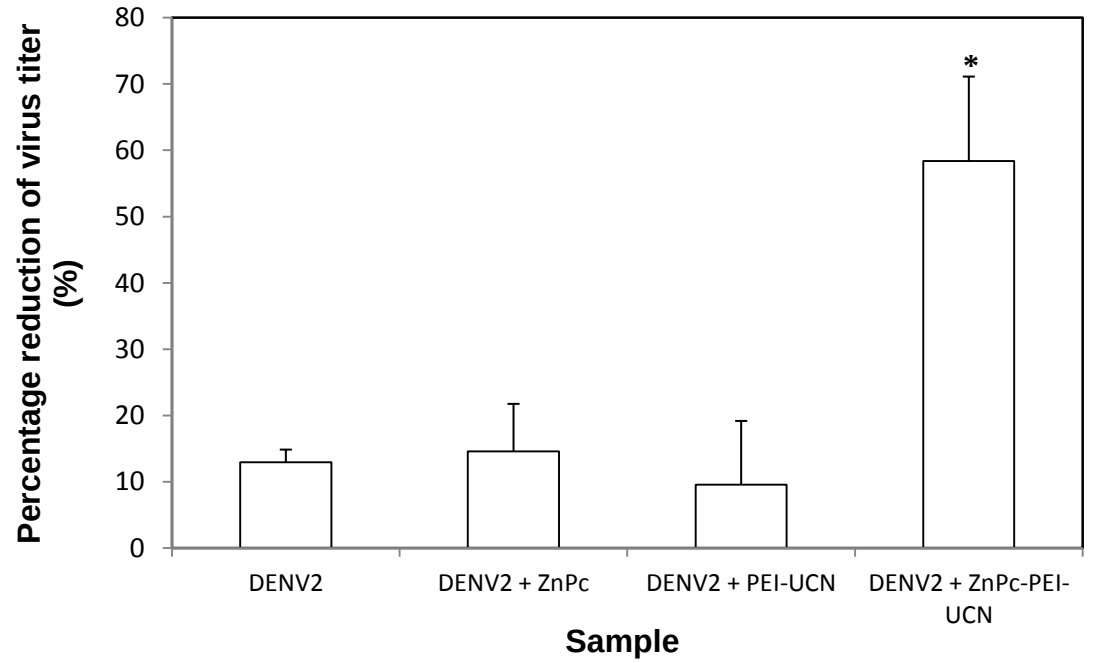

Figure 3.6 Percentage reduction of virus titer for DENV2 irradiated at the fluence of 40 kJ/cm^2 in the presence of 0.1 mM ZnPc photosensitizers, 0.5 mg/mL PEI-UCNs and 0.5 mg/mL ZnPc-PEI-UCNs. Error bars represent standard deviations of the mean. Statistical analysis was done by comparing the samples to the control (the DENV2-only sample) using Student's t-test, ***** $P < 0.05$.

Although photodynamic inactivation effect was not seen on virus suspension samples with PEI-UCNs and ZnPc photosensitizers, a slight reduction in virus titers was observed on samples irradiated at the fluence of 20 kJ/cm^2 and the reduction increased with fluence of 40 kJ/cm^2. This was due to the light photodamage effect of the NIR irradiation. As evidenced from the sample with DENV2 only virus suspension, the virus titer reduction was only 0.22 $\log_{10}$ PFU/mL when irradiated at the fluence of 20 kJ/cm^2 but further increased to around 1 $\log_{10}$ PFU/mL when the fluence was raised to 40 kJ/cm^2. The percentage reduction of virus titer showed a 10% increase from 3% (at 20 kJ/cm^2) to 13% (at 40 kJ/cm^2) for samples with DENV2 only virus suspension. The light photodamage effect was to be expected due to the heat generates from the NIR irradiation. However, it can be deduced from the results that, up to the fluence of 40 kJ/cm^2, the photodamage to DENV2 viruses is negligible as the reduction in virus titers was statistically insignificant.

Overall, this study has demonstrated that PEI-coated UCNs with attached ZnPc photosensitizers is able to photodynamically inactivate viruses and the development of UCN-based photodynamic inactivation system is feasible.

3.3.3 Photodynamic inactivation of DENV2 in suspension

After demonstrating that ZnPc-UCNs were feasible to inactivate viruses, we further explored the UCN-based photodynamic inactivation of viruses in suspension by examining the effect of nanoparticle concentration on photodynamic inactivation efficacy. The ZnPc-PEI-UCNs at various concentrations were mixed with DENV2 and exposed to 980 nm NIR light at the fluence of 14 kJ/cm^2 (as described in Section 3.2.5).

The results showed that there was a concentration-dependent reduction in the infectious DENV2 titers. The infectious titers of DENV2 samples that were irradiated in the presence of the nanoparticles were compared against their respective dark controls, which were samples without NIR irradiation. For all the experimental conditions, photodynamic inactivation efficacy was the least effective using the lowest nanoparticle concentration of 2 μg/mL. Significant reduction in virus titers was observed for nanoparticle concentrations of 4.4, 44 and 440 μg/mL. Compared to their respective dark control samples, virus titers reduced 3.78 $\log_{10}$ PFU/mL (62 % reduction), 4.06 $\log_{10}$ PFU/mL (66 % reduction) and 5.00 $\log_{10}$ PFU/mL (82 % reduction) respectively for these three concentrations (Figures 3.7 and 3.8). However, gradual reduction was observed when nanoparticle concentrations were increased 10-fold from 4.4 μg/mL to 44 μg/mL and finally to 440 μg/mL for the light-treated samples. Virus titer of the light-treated sample of 44 μg/mL was recorded at 2.3 $\log_{10}$ PFU/mL and 1.1 $\log_{10}$ PFU/mL for 440 μg/mL. Although there was an increase of 100-fold in concentration, virus titer reduction of only 1.2 $\log_{10}$ PFU/mL was observed. This could be due to the dislodgment of ZnPc from the surface of the nanoparticles. As ZnPc photosensitizers were only adsorbed physically to the surface of the PEI-UCNs, frictions between the nanoparticles and the interaction of PEI-UCNs with the microenvironment of cell culture medium could result in ZnPc being detached from the nanoparticles easily, thus lowering the photodynamic inactivation efficacy.

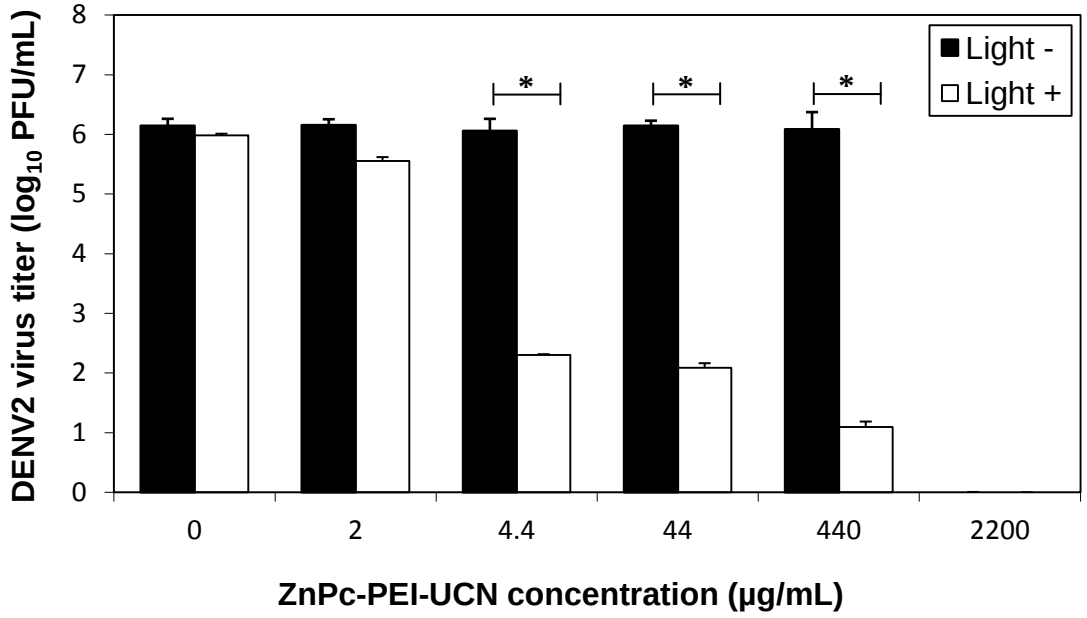

Figure 3.7 Infectious virus titers of DENV2 mixed with different ZnPc-PEI-UCN concentrations and exposed to 980 nm NIR light at the fluence of 14 kJ/cm^2. All experiments were performed in triplicate and error bars represent standard deviations of the mean. Statistical analysis was done by comparing light-treated samples to their respective dark controls using Student's t-test, ***** $P < 0.05$.

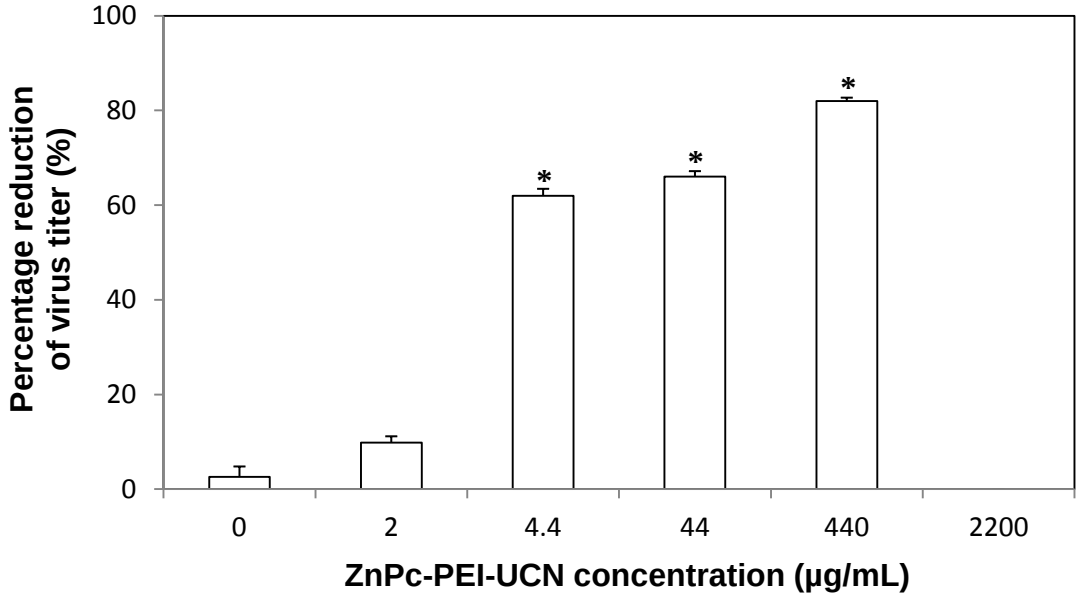

Figure 3.8 Percentage reduction of virus titer for DENV2 irradiated with different ZnPc-PEI-UCN concentrations at the fluence of 14 kJ/cm2. Error bars represent standard deviations of the mean. Statistical analysis was done by comparing each of the samples to the 0 µg/mL control (DENV2-only sample), using Student's t-test, ***** $P < 0.05$.

On the other hand, DENV2 viruses were completely inactivated at 2200 μg/mL, the highest concentration of ZnPc-UCNs used in this study. The complete inactivation was seen for both NIR-irradiated and dark control samples. The dark controls, which were samples without NIR irradiation, not only acted as controls for the light-treated samples but also served to assess the nanoparticle toxicity on viruses. The results showed that ZnPc-PEI-UCNs were not toxic to viruses for all the concentrations tested except 2200 μg/mL. The virus titers for dark control samples of 2, 4.4, 44 and 440 μg/mL were ranged from 6.06 $\log_{10}$ PFU/mL to 6.16 $\log_{10}$ PFU/mL which did not deviate much from the original virus titer used for this experiment (6.37 $\log_{10}$ PFU/mL). Thus the complete inactivation of viruses as seen for the NIR-irradiated sample at the concentration of 2200 μg/mL was not due to photodynamic action but rather because the nanoparticles were too toxic to the viruses at this concentration as seen from its associated dark control which inactivated the viruses completely.

3.4 Conclusions

In conclusion, the findings from this work demonstrate the feasibility of UCN-based PDT to photodynamically inactivate viruses with advantages over current PDT technique. In order to overcome the problem of ZnPc dislodgment, the current design of ZnPc-PEI-UCN should be further improved to maximize its potential in the development of novel anti-viral strategy.

Chapter 4: Synthesis and characterizations of mesoporous silica-coated UCNs

4.1 Introduction

The UCN-based photodynamic inactivation of viruses has been proven feasible using the PEI-coated $NaYF_4$:Yb^{3+}/Er^{3+} UCNs as shown in the previous chapter. By attaching ZnPc photosensitizer to the PEI-coated UCNs via physical adsorption, significant reduction of virus titer due to photodynamic inactivation effect was achieved. However, this design suffers some setback which might hamper its development for clinical use. As ZnPc photosensitizers were attached to the nanoparticles via physical adsorption, these photosensitizers may not be firmly attached to the nanoparticles and can easily dislodge in the complex biological environment, causing low attachment efficiency. In addition, there is also concern of PEI cytotoxicity [63] which could potentially cause collateral damage to host cells by disruptions to cell membrane (causing necrosis) and mitochondrial membrane (causing apoptosis) [64]. Thus, current design of PEI-coated UCNs needs to be improvised in order to develop a clinically-viable and biocompatible UCN-based PDT system.

Apart from PEI polymer which was being used by our group for UCN-based PDT, polyethylene glycol (PEG) has also been explored by others. Ungun *et al.* [56] has synthesized three-layered nanoparticles consisting of $NaYF_4$: Yb^{3+}/Er^{3+} UCNs as the core, porphyrin photosensitizers as the middle layer and a PEG polymer coat as the outer layer. They have demonstrated high photosensitizer-to-UCN ratio of 1:3 but the PDT efficacy of these UCNs has yet to be proven.

In addition to polymer-based approach, another design utilizes silica as a protective layer in which the photosensitizers are impregnated. Using such a strategy, Zhang *et al.* [57] doped merocyanine-540 photosensitizers into the silica shell of UCNs which were further functionalized with antibodies. However, the release of ROS is hampered by the non-porous silica, thereby resulting in low PDT efficacy.

Based on the shortcomings of our current design and the efforts made by other groups, it seems imperative to synthesize UCNs which are able to carry hydrophobic photosensitizers in complex aqueous biological environment without them being easily dislodged. In addition, the generation and production of ROS must not be hampered by the UCN structure. Mesoporous silica materials offer advantages such as large surface area and porous structures which could act as repositories to store hydrophobic photosensitizers. Moreover, the size of the porous structures is tunable, allowing heterogeneous molecules to be kept in the mesoporous silica structures [65, 66]. Most importantly, the porous structures that encapsulate photosensitizers enable ROS produced from the PDT reactions to be released out from the pores with ease. Besides good solubility in water and organic solvents, silica-coating has been proven to confer several advantages such as being stable in biological buffers, biocompatible and allows easy access for grafting of specific ligands, polymers and biomolecules [67-69], all of which are important for biomedical applications.

In view of the advantages of mesoporous silica, this material was selected to replace PEI as the coating material for the nanoparticles. Here, the UCN consists of an upconversion core of $NaYF_4$:Yb^{3+}/Er^{3+} coated with two layers of silica, the inner layer of amorphous silica and outer layer of mesoporous silica. Subsequently, the ZnPC molecules are loaded into the mesoporous silica (Figure 4.1). Our group has reported the successful synthesis of these

nanoparticles [58]. It is expected that by loading the photosensitizers into porous silica, the release of ROS and oxygen diffusion will not be hampered.

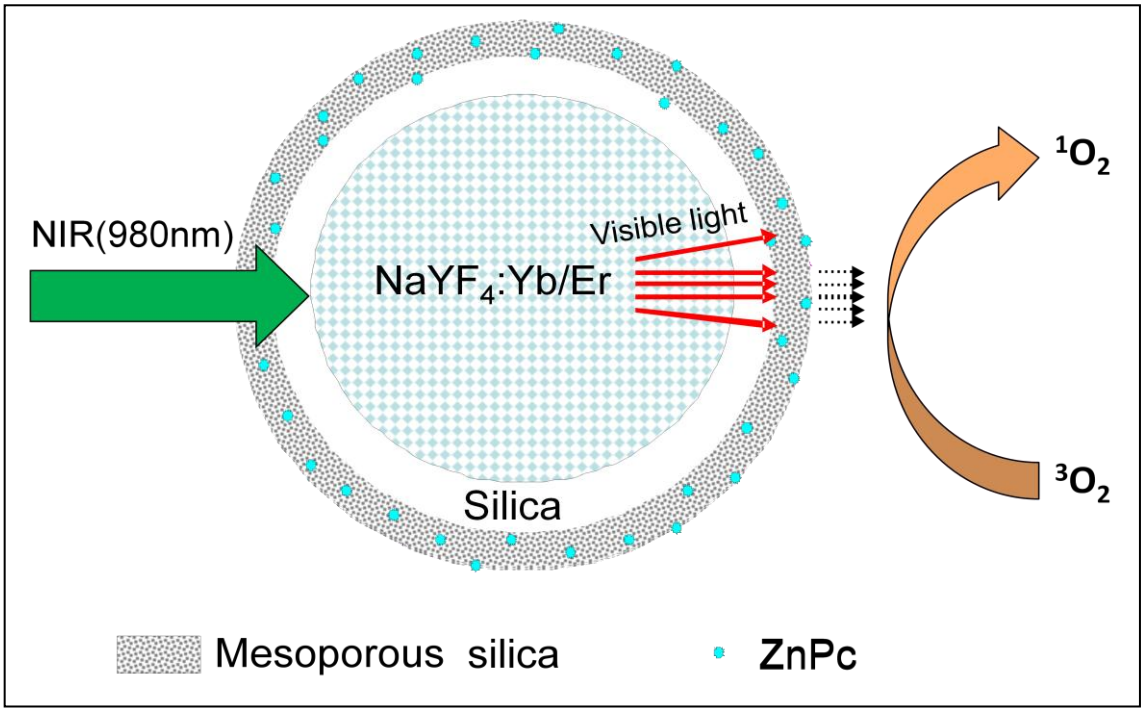

Figure 4.1 Schematic drawing of structure and mechanism of action of mesoporous silica-coated $NaYF_4:Yb^{3+}/Er^{3+}$ nanoparticles loaded with ZnPc photosensitizers.

4.2 Materials and Methods

4.2.1 Materials

Sodium chloride (NaCl, ≥99.0%), yttrium chloride hexahydrate (YCl_3•$6H_2O$, 99.99%), ytterbium oxide (Yb_2O_3, 99.99%), erbium oxide (Er_2O_3, 99.99+%), ammonium fluoride (NH_4F, ≥98%), oleic acid (OA, ≥99%), 1-octadecene (ODE, ≥99.5%), Igepal CO-520, cyclohexane (≥99%), tetraethyl orthosilicate (TEOS, ≥99.9%), ammonia (NH_3, ≥99.9%), methanol, sodium hydroxide (NaOH, ≥97%), acetone (≥99.5%),octadecyltrimethoysilane (C18TMS ≥90%), ammonia hydroxide (NH_4OH, 33%), pyridine (99.8%), dimethyl sulfoxide (≥99.9%), zinc (II) phthalocyanine (ZnPc, 97%) and 9,10-anthracenediyl-bis(methylene) dimalonic acid (ABDA, ≥90%) were purchased from Sigma-Aldrich, USA. Ethanol (EtOH, 89 – 91%) was purchased from VWR International LLC. Phosphate-buffered saline (PBS) was purchased from 1st Base, Singapore.

4.2.2 Synthesis of mesoporous silica-coated $NaYF_4$:Yb^{3+}/Er^{3+} nanoparticles

The mesoporous silica-coated nanoparticles were synthesized with established protocol [58]. It is a three-step process as described below:

Synthesis of $NaYF_4$:Yb^{3+}/Er^{3+} upconversion nanocrystals: 0.8mmol YCl_3, 0.18n mmol $YbCl_3$ and 0.02 mmol $ErCl_3$ were mixed in a 50 mL round-bottom flask with 6 mL OA and 15 mL ODE. In order to form a homogeneous solution, the mixture was heated to 160 ^oC and subsequently cooled to room temperature. 2.5 mmol NaOH and 4 mmol NH_4F in 10 mL methanol was subsequently added and continuously stirred for 30 min. This mixture was heated in a gradual manner in order to eliminate methanol. The mixture was degassed at 100

^{o}C for 10 minutes and flow with Argon for 1 h. After the mixture was cooled down, upconversion nanocrystals were precipitated with ethanol and washed three times with ethanol-water solution.

Silica coating onto the upcvonversion nanocrystals via a microemulsion method: The synthesized upconversion nanocrystals (0.01 M in 4 mL cyclohexane) were mixed with 0.1 mL Igepal CO-520 and 6 mL cyclohexane. The solution was stirred continuously for 10 min followed by the addition of 0.4 mL Igepal CO-520 and 0.08 mL ammonia (30 wt %). After stirring, the flask was sonicated for 20 min in a sealed manner. 0.04 mL TEOS was subsequently added and this flask was shook for 48 h at 600 rpm. After that, acetone was used to precipitate silica-coated nanoparticles and further washed with ethanol-water solution two times before the silica-coated nanoparticles were kept in DI water.

Additional coating of mesoporous silica onto the nanoparticles: A solution containing 100 mL TEOS and 40 μL C18TMS in 20 μL of ethanol was prepared in a round-bottom conical flask before the silica-coated nanoparticles was added to the solution. 1 mL NH_4OH (33%) was further added into the solution and continuously stirred for 6 h at room temperature. Through centrifugation, the nanoparticles were recollected and washed with ethanol and water for 3 times. The nanoparticles were then placed in a furnace and heated at 500 ^{o}C for 6 hours in order to form a mesoporous silica layer on the nanoparticles' surface through the removal of C18TMS.

4.2.3 Characterizations of the nanoparticles

The size and shape of the mesoporous-silica coated nanoparticles were determined by TEM. Nanoparticle solution in a small volume was dropped onto a formvar/carbon-coated grid (300 mesh) and left dried on the bench at room temperature. Samples were then imaged using JEOL 2010 transmission electron microscope with accelerating voltage of 200 kV. The surface charge of the nanoparticles was measured using ZetaSizer NanoZS (Malvern Instruments, UK). 1 mg/mL mesoporous silica-coated nanoparticles in deionized distilled water were filled in a Zeta Cell. This was placed in the ZetaSizer NanoZS chamber and the zeta potential measured. The zeta potential for nanoparticles was measured five times with 30 readings taken for each time. The size distribution of the nanoparticles in solution was studied by dynamic light scattering (DLS) using ZetaSizer NanoZS also. The method and sample preparation were similar as mentioned above. The surface area and pore size distribution of the mesoporous silica-coated nanoparticles were determined by using Quantachrome Nova 2000E Surface Area and Pore Size Analyzer (Quantachrome Instruments, USA). 50mg of the nanoparticles were weighed and added into a sample cell. The sample was vacuum degassed with nitrogen (N_2) flow at 300 ^{o}C for three hours. The purpose of doing this is to remove all the moisture from the sample prior to the actual analysis. Then, the degassed sample was used for analysis. For surface area, a twenty points adsorption and twenty points desorption isotherm was measured while gas adsorption method was used to measure pore size. The UCN's fluorescence emission spectra were measured using SpectroPro 2150i spectrophotometer (Roper Scientific Acton Research , USA) equipped with 980 nm VA-II DPSS laser (PhotoniTech, Singapore). 1 mg/mL of nanoparticles in deionized distilled water was added into a cuvette. The cuvette was then placed in the sample holder of spectrophotometer and the sample was excited by 980 nm

laser (current set at 1.5 mA). The fluorescence emission was measured from 450 nm to 700 nm.

4.2.4. Preparation of ZnPc standard curve

Different ZnPc concentrations (0.4, 0.8, 1.2, 1.6, 2.0, 2.4, 2.8 and 3.25 µg/ml) in pyridine were prepared. 500ul of solution from each concentration sample was added into a cuvette and placed in the sample holder of UV-2450 UV-Visible spectrophotometer (Shimadzu Corporation, Japan). Absorbance at 674 nm for each sample was recorded and these readings against ZnPc concentrations were used to plot the standard curve.

4.2.5 Loading of ZnPc photosensitizers into mesoporous silica of the nanoparticles

A typical loading process involves soaking a certain amount of nanoparticles for 24 h in a pyridine solution containing ZnPc. After soaking, the ZnPc-loaded nanoparticles were recollected by centrifugation and washed 2 times before being kept in L15 cell culture medium for experiments. To determine the ZnPc loading amount, 1 mg mesoporous silica-coated nanoparticles were soaked in 1 mL of different concentrations of ZnPc in pyridine solution (0.2, 0.4, 0.6, 0.8, 1.0, 1.2, 1.4, 1.6 mg/mL) for 24 hours. ZnPc-loaded nanoparticles were obtained by centrifugation and the supernatants were kept for absorbance measurement using UV-2450 UV-Visible spectrophotometer (Shimadzu Corporation, Japan). The absorbance readings at 674 nm were taken and the amount of ZnPc loaded for each sample was calculated based on the ZnPc standard curve.

4.2.6 Determination of singlet oxygen ($^1O_2$) production

Singlet oxygen production was determined by the photobleaching of 9,10-anthracenediyl-bis(methylene)dimalonic acid (ABDA). The ZnPc-loaded nanoparticles obtained from ZnPc loading in different concentrations of ZnPc solution (0.2, 0.4, 0.6, 0.8, 1.0, 1.2, 1.4, 1.6 mg/mL) were used for this purpose. 1 mg of ZnPc-UCN from each ZnPc loading concentration was mixed with ABDA (10 µM) in DI water. The solution was then exposed to 980nm NIR laser at the laser power of 0.47 W for 0, 20, 40, 60 and 80 minutes and the fluorescence intensity of ABDA at 407 nm was measured using SpectroPro 2150i spectrophotometer (Roper Scientific Acton Research, USA). A control sample of 1 mg void UCNs was also exposed to 980 nm NIR laser with the same exposure time. A graph of normalized fluorescence intensity at 407 nm for nanoparticles obtained from different ZnPc loading concentrations against various time points was plotted.

4.2.7 Determination of ZnPc release profile

1mg of ZnPc-loaded nanoparticles was soaked in 1ml of DI water, 1X PBS, pyridine, DMEM, RPMI-1640 and L-15 media respectively for 24 hours. DMEM, RPMI-1640 and L-15 were cell culture media supplemented with 10% fetal bovine serum (FBS). After 24 hours soaking, the nanoparticles were recollected by centrifugation and the supernatants kept for absorbance measurement. UV-Visible absorption spectra of the supernatants were measured using UV-2450 UV-Visible spectrophotometer (Shimadzu Corporation, Japan).

4.3 Results and Discussion

4.3.1 Physical characterizations of mesoporous silica-coated $NAYF_4:Yb^{3+}/Er^{3+}$ nanoparticles

4.3.1.1 Size and shape determinations

TEM can be used for direct determination of size and shape of nanoparticles. Figure 4.2 shows the mesoporous silica layer with thickness of around 11 nm was successfully coated onto the nanoparticles. As revealed by TEM, the porous structures of the mesoporous silica were clearly seen as uneven rough surfaces (Figure 4.2b). Overall, the mesoporous silica coated-$NaYF_4:Yb^{3+}/Er^{3+}$ nanoparticles are spherical in shape and have an average size of 70 nm in diameter.

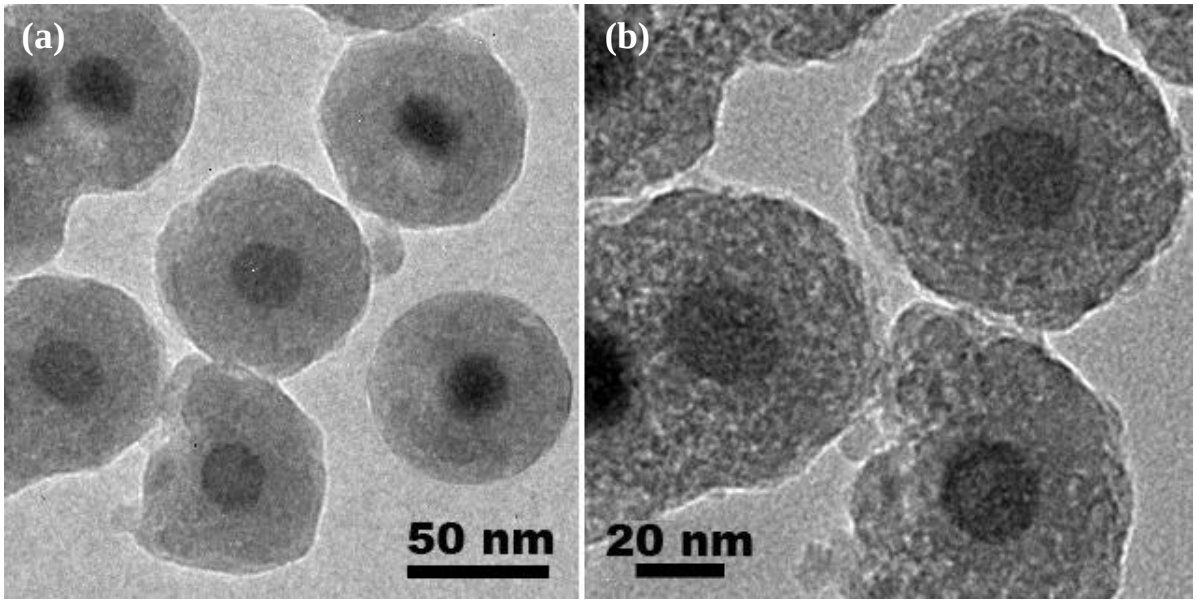

Figure 4.2 (a) TEM images of mesoporous silica-coated $NaYF_4:Yb^{3+}/Er^{3+}$ UCNs. (b) The same nanoparticles at higher magnification showing the porous structures of the mesoporous silica.

4.3.1.2 Quantification of surface charge

The surface charge of a particle in solution is determined by measuring zeta potential. The zeta potential is an illustration of the mean surface charge of the nanoparticles. Surface charge is an important factor in solubility of the nanoparticles in polar solutions. The zeta potential of mesoporous silica-coated $NaYF_4$:Yb^{3+}/Er^{3+} nanoparticles was measured 5 times with an average value of -20.4 mV (Table 4.1). As the nanoparticles' surface was coated with mesoporous silica, the value obtained was consistent and in accordance with the fact that silica has negative surface charge.

Reading	Zeta Potential (mV)
1	-20.7
2	-20.1
3	-20.6
4	-20.4
5	-20.2
Average	**-20.4**

Table 4.1 Zeta potential readings of mesoporous silica-coated $NaYF_4$:Yb^{3+}/Er^{3+} nanoparticles.

4.3.1.3 Size distribution and presence of aggregates

The distribution of nanoparticle sizes determined using DLS provides a valuable indicator of the presence of aggregates in solution. Aggregates of nanoparticles are several times the size of individual nanoparticles and show up as a separate peak in the size distribution graph. The synthesized nanoparticles demonstrated a unimodal size distribution of the nanoparticles with a single peak, (Figure 4.3). It has an average diameter of 127 nm with polydispersity index (PDI) of 0.171. This PDI value corresponds to the monodispersity of nanoparticles in solution

as PDI near 0.1 means that the nanoparticles are monidisperse with narrow size distribution [70] while PDI in the range of 0.5 – 1.0 shows polydispersity of the sample. It is worth to note here that DLS gave an average size of 127 nm in diameter which is bigger than the actual size viewed under TEM. The nanoparticle's size measured using DLS in solution is not the true size but includes the hydrodynamic radius of the layers of water molecules that attached on the nanoparticle's surface. This causes a higher value for size measurement.

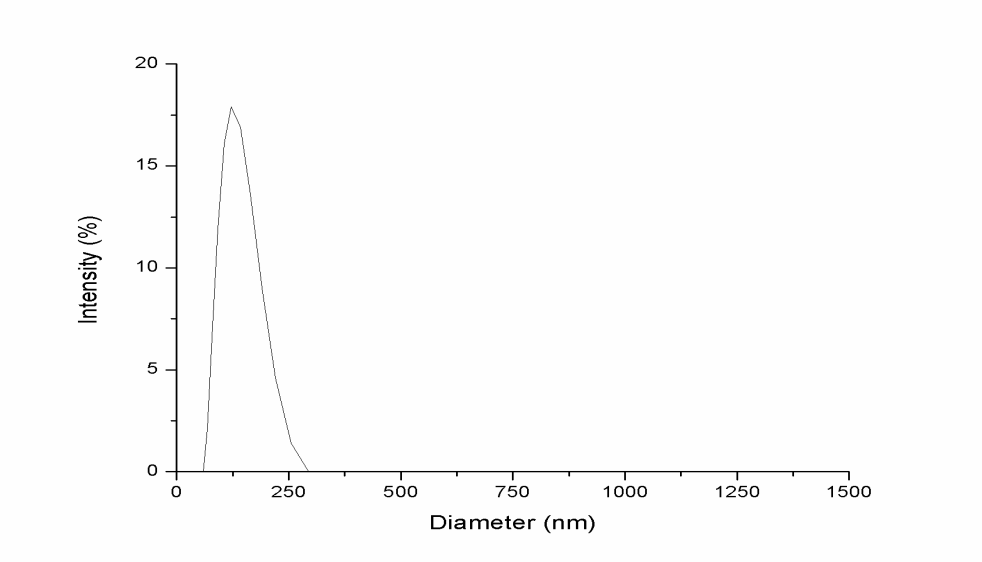

Figure 4.3 Size distribution of mesoporous silica-coated $NaYF_4:Yb^{3+}/Er^{3+}$ nanoparticles in DI water.

4.3.1.4 Surface area and pore size distributions

Based on the adsorption/desorption isotherm of N_2, the surface area of UCNs was measured to be 69.614 m^2/g. The mesoporous silica-coated UCNs have narrow pore size distribution with an average pore size of 3.76 nm in diameter (Figure 4.4). The purpose of degassing the sample with N_2 was to remove all the moisture from the sample prior to the actual analysis.

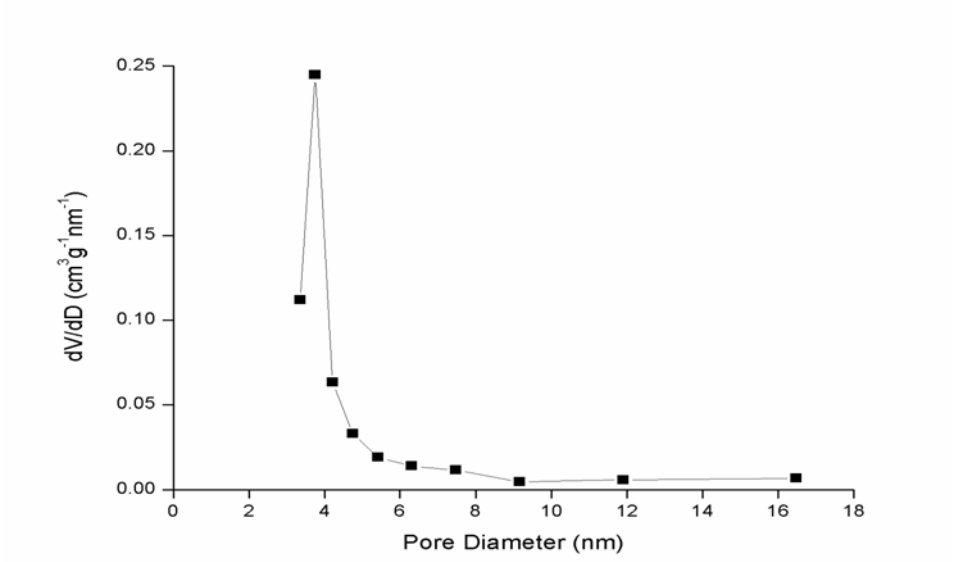

Figure 4.4 Pore size distribution of mesoporous silica-coated $NaYF_4:Yb^{3+}/Er^{3+}$ nanoparticles.

4.3.2 Optical characterization of mesoporous silica-coated $NAYF_4:Yb^{3+}/Er^{3+}$ nanoparticles

Similar to the PEI-coated nanoparticles, the mesoporous silica-coated $NaYF_4:Yb^{3+}/Er^{3+}$ nanoparticles emitted fluorescence in the green and red regions of the visible spectrum with two peaks at 545 nm and 658 nm respectively upon excitation with 980 nm NIR laser (Figure 4.5). The combination of these two peaks gives a resultant emission which appears greenish-yellow.

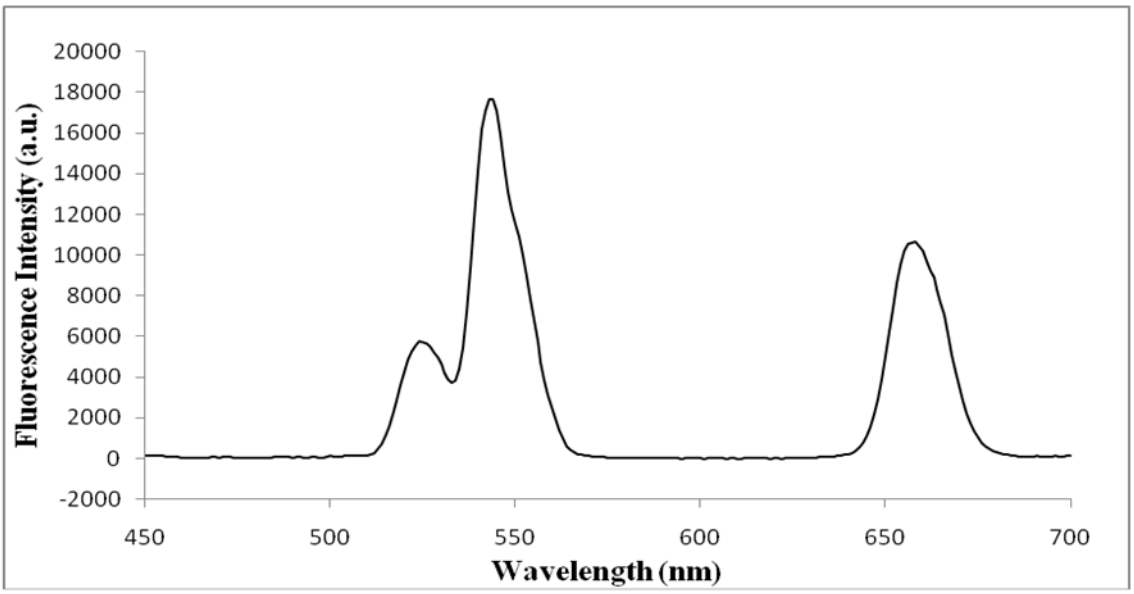

Figure 4.5 (a) Fluorescence emission spectrum of the mesoporous-silica-coated UCN upon excitation at 980 nm.

As mentioned, the mesoporous silica-coated nanoparticles, when excited with NIR laser at 980 nm, emit visible light in green and red regions at 510-570 nm and 640-680 nm respectively. Based on the spectra shown in Figure 4.6, there is a good overlap between the emission spectrum of UCN and absorption spectrum of ZnPc (which peaks at around 674 nm) in the red light region. The overlapping allows ZnPc being encapsulated in the porous silica of the nanoparticles to absorb the visible light emitted by the nanoparticles upon excitation by 980 nm NIR light.

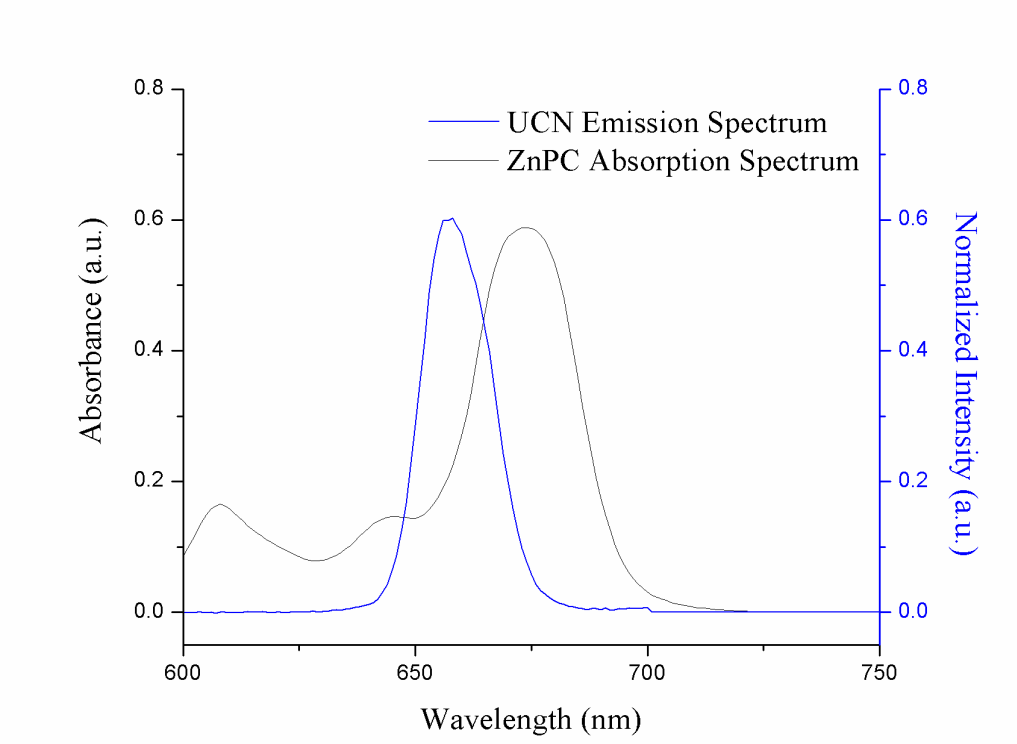

Figure 4.6 Emission spectrum of UCN upon excitation by 980 nm NIR laser (blue) and absorption spectrum of ZnPc (grey) in the red region of visible light.

4.3.3 Loading of ZnPc photosensitizers into mesoporous silica of the nanoparticles

As the generation of ROS and singlet oxygen were mediated by photosensitizers, the amount of ZnPc loaded has a direct implication on the photodynamic inactivation efficacy. It is expected that higher amount of ZnPc produces better photodynamic inactivation efficacy. In order to optimize the amount of ZnPc photosensitizers loaded into mesoporous silica of the nanoparticles, a ZnPc standard curve was first developed based on the UV-Visible absorbance readings of standard ZnPc solutions in pyridine (as described in Section 4.2.4). 1 mg nanoparticles were soaked in 1 mL of different loading concentrations of ZnPc solution for 24 hours. After 24 hours, the nanoparticles were recollected by centrifugation and supernatants were kept for absorbance readings at 674 nm, which is the absorption maximum of ZnPc. The supernatants corresponded to free or unloaded ZnPc photosenstitizers that were

not incorporated into mesoporous silica of the nanoparticles. Based on the absorbance readings at 674 nm, the amount of ZnPc photosensitizers in the supernatants were calculated from the ZnPc standard curve. The amount of ZnPc photosensitizers loaded into the mesoporous silica shell could then be obtained from the subtracted value of the amount of ZnPc in the supernatant from the initial ZnPc loading amount. As the nanoparticles were soaked in 1 mL of ZnPc solution, the initial ZnPc loading amounts used correspond to their respective ZnPc loading concentrations. For example, 0.2 mg or 200 μg was the initial loading amount for the ZnPc loading concentration of 0.2 mg/mL.

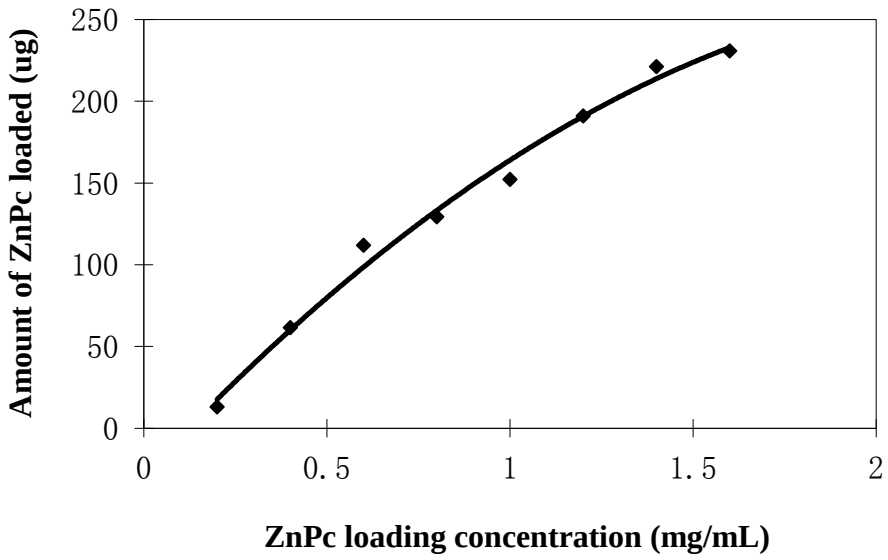

Figure 4.7 Amount of ZnPc photosensitizers loaded into the mesoporous silica-coated nanoparticles which were soaked with various ZnPc loading concentrations.

Based on the results obtained (Figure 4.7), it was observed that the amount of ZnPc photosensitizers loaded into the mesoporous silica-coated nanoparticles increased with ZnPc loading concentration. Higher ZnPc loading concentration will result in more photosensitizers being loaded into mesoporous silica of the nanoparticles. 13 μg of ZnPc photosensitizers were being loaded into mesoporous silica using the lowest ZnPc concentration of 0.2 mg/mL (initial ZnPc loading amount of 0.2 mg) while the highest ZnPc loading concentration of 1.6 mg/mL resulted in 230 μg of ZnPc photosensitizers being loaded into porous silica of the

nanoparticles. Loading efficiency was calculated as the percentage of ZnPc loaded amounts against their respective initial loading amounts. For the fixed amount of nanoparticles (1 mg) soaked in all ZnPc loading concentrations except 0.2 mg/mL, the loading efficiency was about the same in the range of 14 – 18 % of their initial loading amounts. The loading efficiency for 0.2 mg/mL ZnPc loading concentration (initial loading amount of 0.2 mg) was merely 6.52 %. Overall, the optimum loading amount of ZnPc photosensitizers could not be determined as the saturation point or plateau was not observed in this study. Higher ZnPc loading concentrations could be used to further increase the amount of loaded ZnPc photosensitizers until a saturation point or plateau was reached.

4.3.4 Determination of ZnPc loading by singlet oxygen profile via ABDA assay

Although the optimum loading amount of photosensitizers was not determined from the previous experiments, studies have suggested that higher amount of photosensitizers do not necessary brings better photodynamic effect. There were reports of aggregation-induced photosensitizer self-quenching which could lead to reduce photosensitivity and photoactivity. This quenching effect is due to aggregation of photosensitizers when high amount of photosensitizers is being used. The aggregation causes self-quenching of the fluorescence and photoactivity of neighboring photosensitizers, leading to a much reduced ROS generation. This quenching phenomenon was also being observed upon the encapsulation of photosensitizers into polymeric nanoparticles using two different photosensitizers, porphyrins and chlorins [71]. Aggregation-induced quenching was described when silicon phthalocyanine (SiPc) was encapsulated into polymeric micelles [72]. ZnPc is also affected by self-quenching effect as fluorescence quenching was observed when ZnPc of high

concentrations was incorporated into the liposome carrier system [73]. Thus, compare to determining the loading amount of ZnPc photosensitizers, it seems more reasonable to optimize the ZnPc loading through singlet oxygen profiles of ZnPc-loaded mesoporous silica-coated nanoparticles (ZnPc-MS-UCNs) which were obtained from ZnPc solutions of different loading concentrations.

The production and release of singlet oxygen is the most crucial step in the photodynamic action of photosensitizers by converting molecular triplet oxygen to singlet oxygen, thereby catalyzing the inactivation of viruses. The production and release of singlet oxygen from the mesoporous silica-coated nanoparticles were investigated in this study via the photobleaching of 9,10-anthracenediyl-bis(methylene)dimalonic acid (ABDA). $^1O_2$ reacts with ABDA and produces endoperoxide, thereby causing a decrease in the amount of ABDA. Hence, the decrease in ABDA fluorescence intensity is inversely proportionate to the increase in singlet oxygen production. The fluorescence intensity of ABDA can be measured at 407 nm, which is the emission maximum of ABDA.

As shown in Figure 4.8, the results demonstrated time-dependent decrease of ABDA fluorescence intensity, indicating an increase in the production of singlet oxygen over time by ZnPc-MS-UCNs. More singlet oxygen was produced as the rate of singlet oxygen production was rapid in the first 20 minutes of NIR irradiation. This was evidenced from the ABDA fluorescence intensity which reduced notably in the first 20 minutes and stabilized after that. The singlet oxygen profiles showed that higher ZnPc loading concentrations did not result in better singlet oxygen production efficiency. This is in consistent with the above-mentioned aggregation-induced self-quenching effect of photosensitizers. The ABDA fluorescence intensity remained unchanged over time for nanoparticles soaked in ZnPc loading

concentration of 1.2 mg/mL and was even higher than the control sample of void UCNs which showed a very minute reduction in the ABDA fluorescence intensity. Upon comparison of all the singlet oxygen profiles, the singlet oxygen profile of nanoparticles soaked in ZnPc loading concentration of 0.8 mg/mL showed the highest decrease in ABDA fluorescence intensity over time which correlates to the highest amount of singlet oxygen being produced. This loading concentration was used for subsequent ZnPc loading in preparation of ZnPc-MS-UCNs for photodynamic inactivation experiments. Based on the previous study, the ZnPc loading amount of nanoparticles soaked in 0.8 mg/mL ZnPc solution was around 130 µg. Thus, this amount was regarded as the optimum ZnPc loading amount.

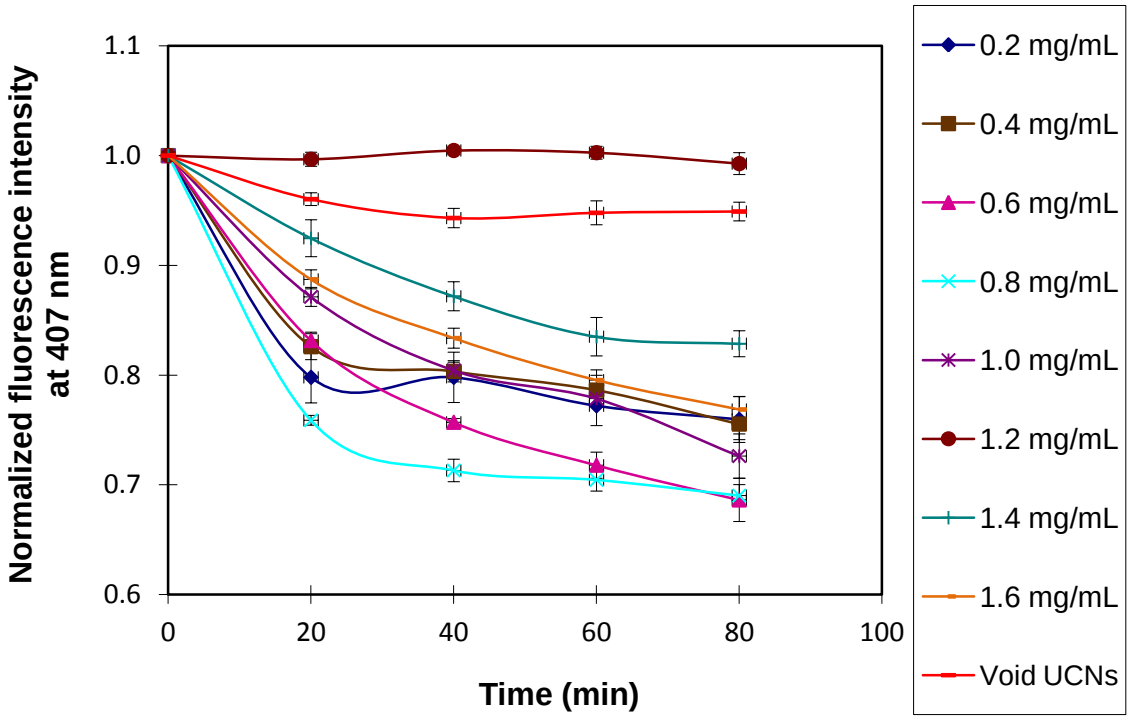

Figure 4.8 Singlet oxygen profiles of ZnPc-MS-UCNs soaked in various ZnPc loading concentrations. The production of singlet oxygen was determined via ABDA destruction assay. All experiments were performed in triplicate and error bars represent standard deviations of the mean.

After ZnPc photosensitizers have been loaded into mesoporous silica of the nanoparticles, the nanoparticles changed from white color to blue-green color, indicating the incorporation of ZnPc photosensitizers into the mesoporous silica (Figure 4.9).

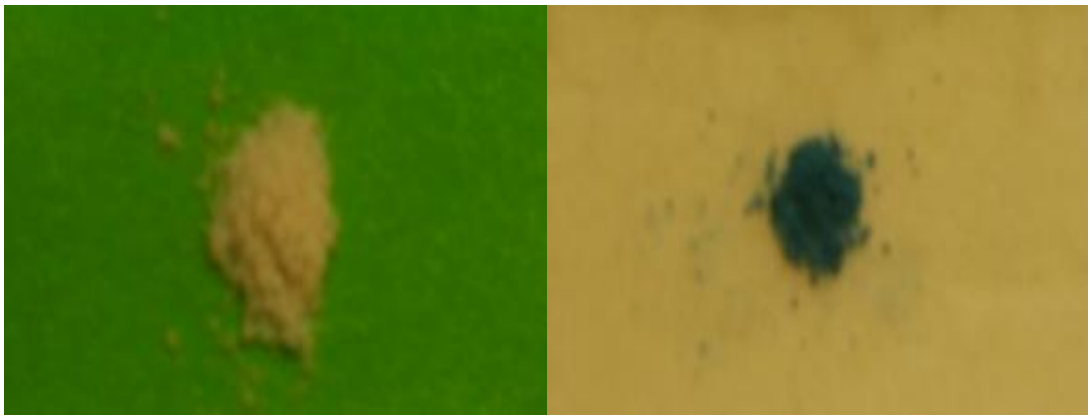

Figure 4.9 Photographs of mesoporous silica-coated $NaYF_4:Yb^{3+}/Er^{3+}$ nanoparticles (a) before (white) and (b) after (blue-green) soaking in ZnPc solution.

4.3.5 ZnPc release profile in aqueous solutions

It is imperative that ZnPc remains intact inside the mesoporous silica of the nanoparticles in aqueous biological environment to ensure the continuous singlet oxygen production upon exposure to NIR light. Thus, the release profile of ZnPC in various aqueous solutions was investigated. As described in Section 4.2.7, the ZnPc-MS-UCNs were soaked in different solutions for 24 hours. The nanoparticles were recollected via centrifugation and supernatants were kept for absorbance measurements. The supernatants correspond to ZnPc photosensitizers that were being leached out from the porous silica of nanoparticles. The findings demonstrated that ZnPc molecules were being leached out from the mesoporous silica in pyridine but was retained in the porous structure in DI water, PBS and cell culture media (Figure 4.10). These findings indicated that ZnPc photosensitizers would remain intact in the mesoporous silica after loading and not leaching out when incubated in cell culture media, PBS or DI water.

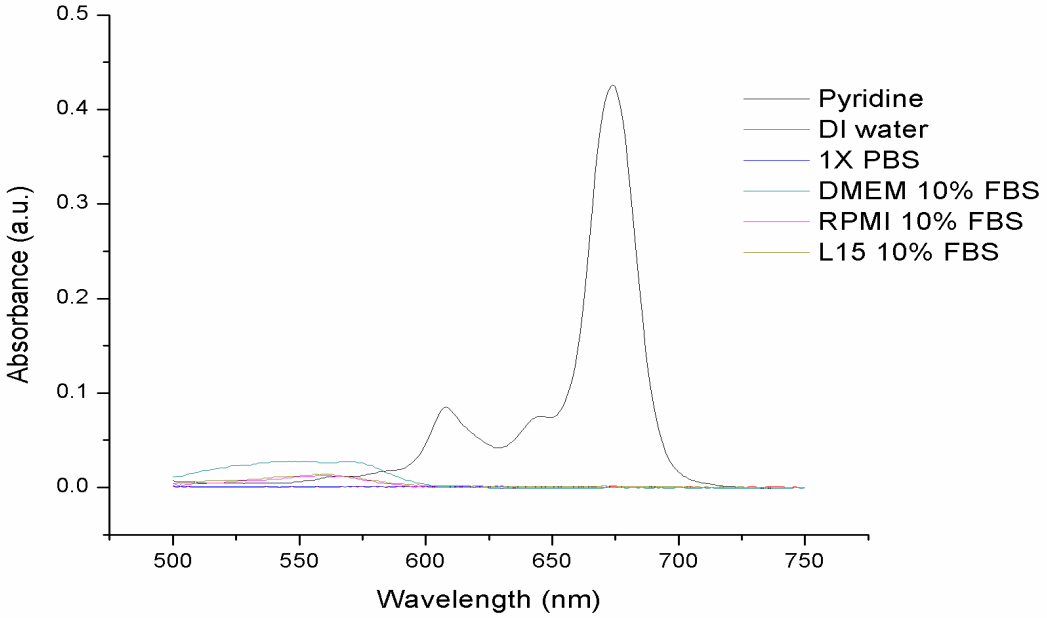

Figure 4.10 ZnPc release profile of ZnPc-MS-UCNs soaked in pyridine, DI water, 1X PBS and cell culture media.

4.4 Conclusions

We report here the synthesis and characterizations of mesoporous silica-coated $NaYF_4:Yb^{3+}/Er^{3+}$ nanoparticles. These nanoparticles possess mesoporous silica to store photosensitizers. The porous structures of silica ensure that singlet oxygen can be released from the pores to the microenvironment with ease. The hydrophobic photosensitizers remain intact in the pores when incubated in aqueous solutions. Porous silica protects photosensitizers from being degraded in the harsh and complicated biological environment. The photosensitizer-loaded nanoparticles are reusable by soaking the particles in pyridine solution.

Chapter 5: Mesoporous silica-coated UCNs for photodynamic inactivation of viruses

5.1 Introduction

The mesoporous silica-coated $NaYF_4$:Yb^{3+}/Er^{3+} nanoparticles have been synthesized in our group with established protocol [58] and well-characterized with many improved features for ZnPc loading as mentioned in the previous chapter. These nanoparticles have been used in our group for PDT of bladder cancer cells [58] and the cytotoxic effect via singlet oxygen-induced apoptosis was demonstrated. Additionally, production of singlet oxygen from these ZnPc-MS-UCNs in live cells has been proven [59].

In this chapter, the photodynamic inactivation efficacy of ZnPc-MS-UCNs to inactivate DENV2 in suspension was discussed. On the other hand, similar experimental settings were carried out in the presence of mouse tissues in order to investigate the ability of NIR light to penetrate mouse tissues of a certain thickness to inactivate the viruses in suspension beneath the tissues. Current light sources used in clinical settings have limited tissue penetration ability which confines their application only to treat superficial lesions and warts. Patients are told not to expose their treated area to sunlight so as to avoid further excitation of photosensitizers that could harm the healthy cells of the treated area. One of the advantages of employing UCNs in this instance is its unique optical properties to be excited by light of longer wavelength and produce higher energy emissions with shorter wavelength. Generally, longer wavelengths have the ability to penetrate deeper into tissue than light with shorter wavelengths. Thus, these nanoparticles when diffuse into the tissues could utilize the NIR light to inactivate viruses beneath the skin in order to achieve complete virus inactivation outcome. The use of NIR light also circumvents the problem of exposure to sunlight or

visible light after treatment as the photodynamic actions of these UCNs will only occur upon excitation by NIR light.

5.2 Materials and Methods

5.2.1 Materials

Roswell Park Memorial Institute-1640 (RPMI-1640) medium, L-15 medium (Leibovitz), crystal violet and methanol were purchased from Sigma-Aldrich, USA. Fetal bovine serum (FBS) and penicillin-streptomycin were purchased from PAA Laboratories GmbH, Austria. Trypsin-EDTA (0.5% Trypsin with EDTA•4Na) was purchased from GIBCO Invitrogen, USA. Phosphate-buffered saline (PBS) was purchased from 1st Base, Singapore. Sodium bicarbonate ($NaHCO_3$) and formaldehyde (37%) were purchased from Merck KGaA, Germany. Carboxymethylcellulose (CMC) sodium salt (Aquacide II) was purchased from EMD Chemicals, USA. All of the reagents were used as received without further purification. Mouse skin tissues of female C57BL/6 mice, 4 – 6 weeks old were obtained from Ms. Niagara Muhammad Idris with approval from the NUS Institutional Animal Care and Use Committee (IACUC).

5.2.2 Cell culture

BHK-21 and C6/36 cell lines were cultured and used for different experiments. BHK-21 cells were cultured in RPMI-1640 medium while C6/36 cells were cultured in L15 medium. All the cell culture media were supplied with FBS and penicillin-streptomycin as antibiotics. For L15 medium, FBS was heat inactivated at 56 ^{o}C for 30 min before being added into the medium. Cell culture media that were supplemented with 10% FBS were used as growth media for the cell lines while cell culture media with 2% FBS were used as maintenance

media to enable cell survival. The pH of RPMI-1640 media were adjusted to the range of 7.2 – 7.4 with sodium bicarbonate. All the cells, except C6/36 cells, were cultured in 75 cm^2 flasks and incubated in a humidified incubator with 5% CO_2 at 37 ^oC. C6/36 cells were incubated in dry incubator without CO_2 at 28^oC.

Cells were sub-cultured from confluent monolayer. The cell culture medium was first discarded and the cell monolayer was washed with 5 mL of PBS. 2 mL of trypsin was then added and the flask was placed in an incubator for 3 - 5 min at 37 ^oC to detach the cells from the flask. 8 mL of cell culture medium was added to the cell suspension to neutralize the enzymatic activity of trypsin. Multiple pipetting of the cell culture medium resulted in a single cell suspension. An appropriate amount of cells was re-seeded in the flask and the rest of the cells were discarded. The flask was then incubated in an incubator at an appropriate temperature. Cell monolayer that reaches confluency in 3 to 4 days was used for experiments.

To seed a certain amount of cells for experiments, cell counting using hemocytometer was used. The hemocytometer and glass coverslip were first cleaned with 70 % ethanol. The coverslip was placed over the hemocytometer surface at a height of 0.1 mm so that the total volume for each of the nine 1 mm^2 squares of the counting grid is 0.1 mm^3. After trypsinization, one drop of cell suspension was introduced into one of the V-shaped wells with a micropipette and the area under the coverslip was filled by cell suspension due to capillary action. The hemocytometer was then placed on a microscope stage and the counting grid was observed under 10X objective using a brightfield microscope. The cells in the four corner squares were counted. Only the cells on the top and left-hand sides of each square were included to avoid bias. Cell concentration was calculated as follows:

$$\text{Cell concentration (cells/mL)} = \text{Average number of cells per square} \times 10^4$$

5.2.3 Preparation of DENV2 virus stock

The virus used was Dengue virus serotype 2 (DENV2, New Guinea C strain) which was propagated on C6/36 cells. The cell culture medium was discarded and the cell monolayer was rinsed with 5 mL of PBS. Multiplicity of Infection (M.O.I.) of 10 was used. 1 mL of virus suspension was used for the infection of cell monolayer in a 75cm^2 flask. The flask was incubated at 37 ^{o}C for 1 h and rocked every 15 min to ensure even infection of the whole flask. After 1 h, 14 mL of maintenance medium was added to the flask. The cells were incubated at 28 ^{o}C until the cytopathic effects of the respective cell lines became pronounced. DENV2 was harvested after 4 days of incubation, when syncytial formation on C6/36 cells was completed. To harvest the viruses, the extracellular virus-containing supernatants were collected and spun at 1500 rpm for 10 minutes to remove cellular debris. The virus supernatants were then aliquoted into sterile cryovials, sealed and immediately stored at -80 ^{o}C.

5.2.4 Plaque Assay

The amount of viruses harvested was determined and the virus titer, which is the concentration of infectious viral particles, was calculated. Ten-fold serial dilutions of the DENV2 samples up to the dilution factor of 10^{-6} were prepared in maintenance media of RPMI 2 % FBS. Aliquots of 100 µL from the appropriate dilutions were inoculated in triplicates onto monolayers of confluent BHK-21 cells grown in sterile 24-well tissue culture plate (plated at 62,500 cells/well). The virus-inoculated monolayers were incubated for 1 h at 37 ^{o}C and rocked every 15 min to ensure even distribution of virus inocula. After 1 h of incubation, the inocula were removed upon washing thrice with PBS. 1 mL of semi-solid medium, 2 % carboxymethylcellulose (CMC) in cell culture medium containing 2 % FBS,

was then layered onto the virus-infected cell monolayers. The plates were incubated at 37 ^{o}C in a humidified incubator with 5 % carbon dioxide for five days. After incubation, circular zones of infected cells called plaques were formed. Plaques were visualized by staining the cell monolayer with 0.5 % crystal violet solution overnight at room temperature. Plaques were counted and only wells in the range of between 10 and 100 plaques were accounted for in order to minimize error. Number of plaques counted, in combination with the dilution factor from which the plaques were counted were used to calculate the virus titer, expressed as plaque-forming units per millilitre (PFU/mL). PFU values indicate the number of infectious virus particles for a particular sample with an assumption that a single plaque represents an infectious virus particle.

5.2.5 NIR light attenuation study

A black box was used for this study (Figure 5.1). Holes were created at two opposite sides large enough to hold the 980 nm VD-IIIA DPSS NIR laser driver (Photonitech, Singapore) and NIR detector (model no. NIR512, Ocean Optics, USA). The NIR detector was connected to a computer installed with Spectrasuite software (Ocean Optics, USA) for recording of NIR intensity. A cuvette was placed at the centre of the box and a cuvette holder made from polystyrene was used to hold the cuvette firmly on its ground. NIR filter was sticked to the cuvette's surface at the side facing the NIR detector. 3 mL of sample solution was added into the cuvette and irradiated at a certain laser power. The NIR light that passed through the solution was detected by NIR detector. The NIR intensity between 950 nm and 1000 nm was recorded by Spectrasuite software (Ocean Optics, USA). To measure the NIR intensity of sample solution in the presence of tissues, mouse skin tissues of 1 mm thick from the mice's back of female C57BL/6 mice, 4 – 6 weeks old were used. The thickness of the skin tissues

was measured with vernier caliper in order to ensure that the skin tissues used were of uniformly 1 mm thick. 3 different tissue thicknesses at 1, 5, and 10 mm were tested. For tissue thickness of 5 mm, 5 pieces of mouse skin tissues, each at 1 mm thick were stacked together and the same applied to tissue thickness of 10 mm with 10 pieces of 1 mm thick mouse skin tissues. The tissues were stuck to the cuvette at the side facing the NIR laser driver. The sample in the presence of tissues was irradiated by NIR laser at a certain laser power. The NIR light that passed through the tissues and the solution was detected by NIR detector and the NIR intensity between 950 nm and 1000 nm was recorded. The samples tested and experimental conditions used in this study were shown in Table 5.1.

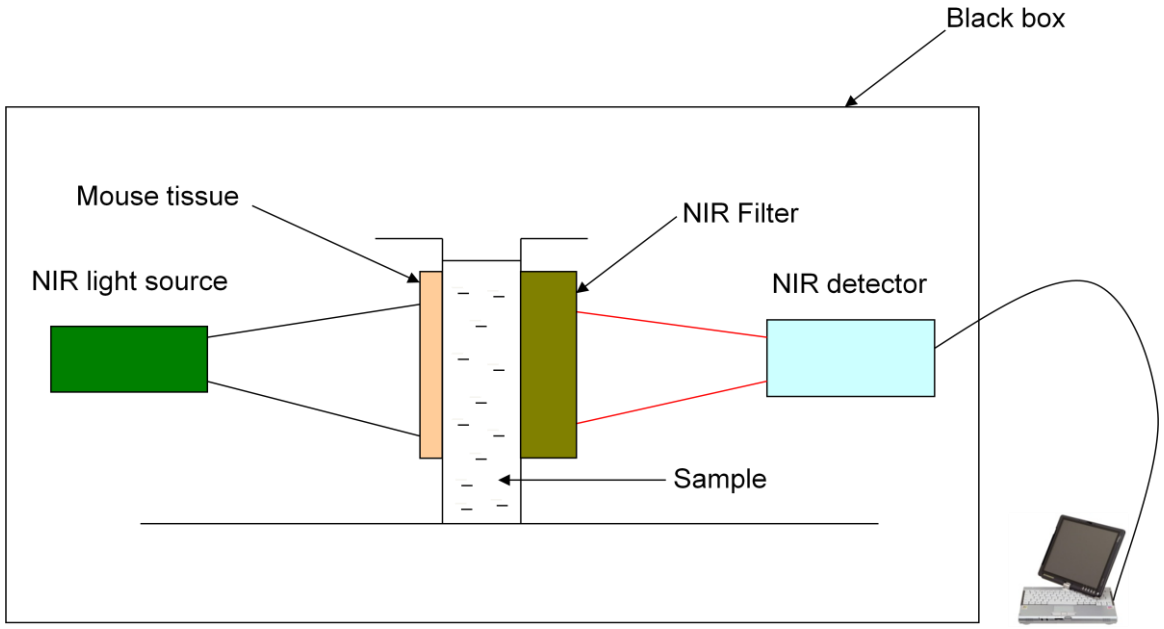

Figure 5.1 Experimental design for light attenuation study.

Sample		Laser Power
DI water	Without mouse tissue	Each sample was irradiated with five different laser powers at 68.7, 470, 660, 858 and 1150 mW
L15 medium		
L15 + ZnPc-MS-UCN		
L15 + ZnPc-MS-UCN + DENV2		
L15 + ZnPc-MS-UCN + DENV2	With mouse tissue (Thickness: 1 mm)	
L15 + ZnPc-MS-UCN + DENV2	With mouse tissue (Thickness: 5 mm)	
L15 + ZnPc-MS-UCN + DENV2	With mouse tissue (Thickness: 10 mm)	

Table 5.1 Experimental conditions for NIR light attenuation study. The concentration of ZnPc-MS-UCN was 1 mg/mL and DENV2 titer was 2.59 x10^7 PFU/mL.

5.2.6 NIR light photodamage to DENV2

200 µL DENV2 (7.41 $\log_{10}$ PFU/mL) was irradiated with NIR light at 980 nm VD-IIIA DPSS NIR laser driver in a 96-well tissue culture plate. Different light fluences of 20, 40, 80 and 160 kJ/cm^2 were tested and the distance between the light source and the viral samples was set at 5 cm. Another similar set of samples were prepared as dark controls, they were not subjected to NIR irradiation but kept in the dark for the same duration as the NIR irradiation time of the light-treated samples. Virus titers of all the samples were determined by plaque assay as described in Section 5.2.4.

5.2.7 Photodynamic inactivation of DENV2 in suspension

200 µL of DENV2 (7.41 $\log_{10}$ PFU/mL) in L15 medium were mixed with a range of ZnPc-MS-UCN concentrations (0, 100, 500, 750, 1000, 1250, 1500, 2000 µg/mL) in a 96-well tissue culture plate under aseptic conditions. These samples were irradiated with NIR light at 980 nm using VD-IIIA DPSS NIR Laser Driver at the fluence of 20 kJ/cm^2 (with laser power of 0.47 W and irradiation time of 14 min 11 sec) with the distance between the light source and the viral samples fixed at 5 cm. A similar set of samples were also prepared and they were kept in the dark for the same duration as the NIR irradiation time of the light-treated samples. Virus titers of the light-treated and dark control samples were determined via plaque assay as described in Section 5.2.4.

In another study, 200 µL of DENV2 (7.41 $\log_{10}$ PFU/mL) in L15 medium were mixed with 0.5 mg/mL ZnPc-UCNs in a 96-well tissue culture plate under aseptic conditions. The samples were exposed to NIR irradiation at 980 nm using VD-IIIA DPSS NIR laser driver at different light fluences (20, 30, 40, 50, 60 kJ/cm^2). The laser power was fixed at 0.47 W and

various irradiation time depending on the light fluences were used (Table 5.2). The distance between the light source and the viral samples was fixed at 5 cm. Another similar set of samples were prepared but they were kept in the dark for the same duration as the NIR irradiation time of the light-treated samples. Virus titers of the light-treated and dark control samples were determined via plaque assay as described in Section 5.2.4.

Light fluence (kJ/cm^2)	**Irradiation time**
20	14 min 11 sec
30	21 min 17 sec
40	28 min 22 sec
50	35 min 28 sec
60	42 min 33 sec

Table 5.2 Experimental conditions for photodynamic inactivation of viruses at different light fluences and the associated irradiation time.

For both the studies, reduction in virus titers was obtained by subtracting the virus titers of the NIR light-treated samples from the virus titers of their associated dark controls. Photodynamic inactivation efficacy was assessed based on percentage reduction of virus titer. Percentage reduction of virus titer was calculated based on the formula given below:

$$\text{Percentage reduction of virus titer (\%)} = \frac{\text{Virus titer of dark control sample (Light -)} - \text{Virus titer of light-treated sample (Light +)}}{\text{Virus titer of dark control sample (Light -)}} \times 100\ \%$$

5.2.8 Photodynamic inactivation of DENV2 in the presence of mouse tissues

200 µL of DENV2 (7.41 $\log_{10}$ PFU/mL) in L15 medium were mixed with a range of ZnPc-MS-UCN concentrations (0, 100, 500, 750, 1000, 1250, 1500, 2000 µg/mL) in a 96-well tissue culture plate under aseptic conditions. The wells were covered with mouse skin tissues of 5 mm thick (Figure 5.2). This was achieved by stacking 5 pieces of 1 mm thick mouse skin tissues as described in Section 5.2.5. These samples were then irradiated with NIR light at 980 nm using VD-IIIA DPSS NIR Laser Driver at the fluence of 40 kJ/cm^2 (with laser power of 0.284 W and irradiation time of 46 min 57 sec) and the distance between the light source and the viral samples was fixed at 5 cm. A similar set of samples were also prepared and they were kept in the dark covered with 5 mm mouse skin tissues for the same duration as the NIR irradiation time of the light-treated samples. Virus titers of the light-treated and dark control samples were determined via plaque assay as described in Section 5.2.4. Reduction in virus titers was obtained by subtracting the virus titers of the NIR light-treated samples from the virus titers of their associated dark controls. Photodynamic inactivation efficacy was assessed based on percentage reduction of virus titer as described in Section 5.2.7.

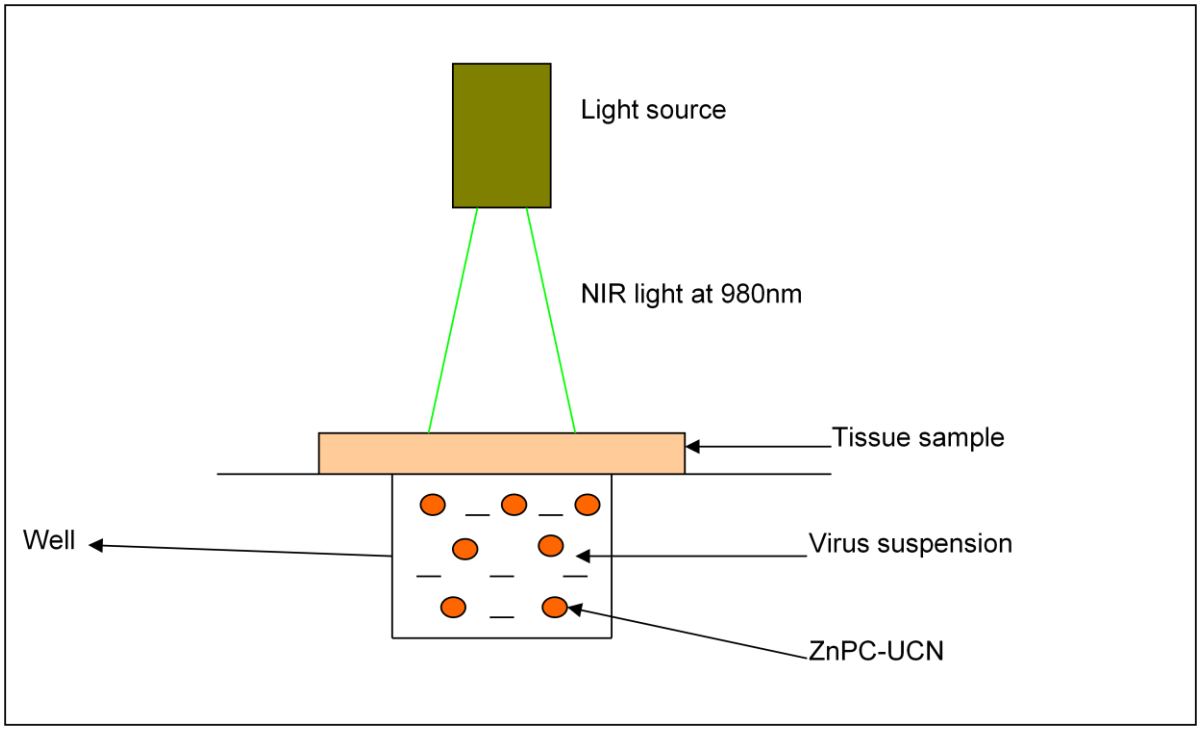

Figure 5.2 Experimental design for photodynamic inactivation of DENV2 in suspension beneath mouse skin tissues.

5.3 Results and Discussion

5.3.1 NIR light attenuation of DENV2, UCNs and cell culture medium

A light attenuation study was done to investigate any possible interference the different components of a sample have on NIR light propagation. The interference could be due to absorption or scattering of the NIR light by the components of a sample which in turn reduces the energy to excite the photosensitizers and subsequently weaken the photodynamic inactivation efficacy. A typical sample consists of DENV2 and ZnPc-MS-UCNs in L15 cell culture medium. A sample containing only L15 medium was tested for the NIR light attenuation before nanoparticles and DENV2 were being added subsequently. A DI water sample was introduced as a control. Five laser powers from lower to higher ends were used in this study. As shown in Figure 5.3, only one intensity peak at 980 nm was obtained which is in accordance with the NIR laser driver designed to emit NIR light at the wavelength of 980 nm. NIR intensities of L15 medium, L15 medium with nanoparticles and L15 medium containing nanoparticles and DENV2 remained stable for all five laser powers tested. All the samples including DI water displayed similar intensities when they were exposed to NIR irradiation. It can be concluded from this study that NIR light was not attenuated by components of a typical sample used for photodynamic inactivation experiments and the light energy delivered to the sample remained stable.

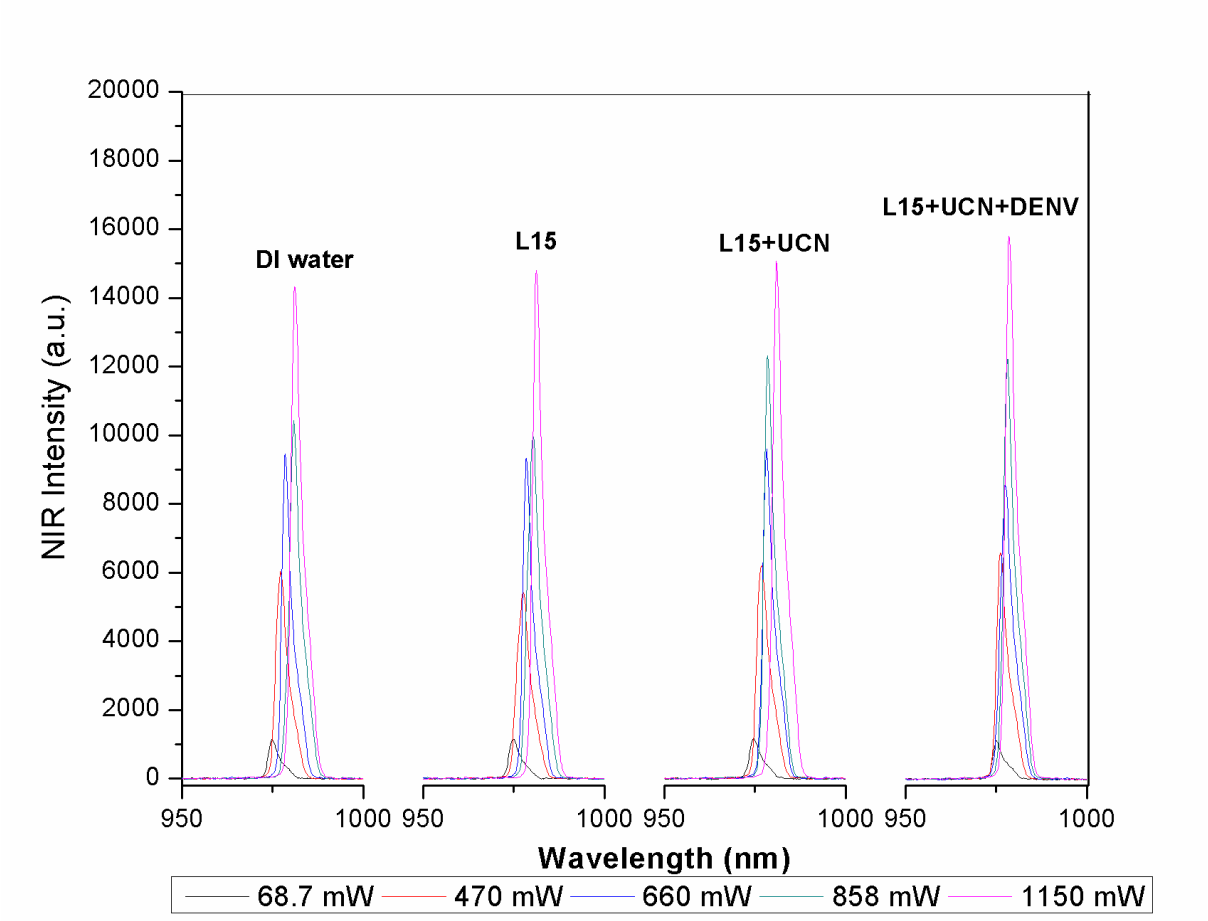

Figure 5.3 NIR intensities that passed through different components in a typical sample used for photodynamic inactivation experiments. DI water was used as a control.

5.3.2 Background study on NIR light photodamage to DENV2

Before commencing the studies on the photodynamic inactivation efficacy of ZnPc-MS-UCNs, it was imperative to examine NIR light photodamage to viruses. Light irradiation normally produces heat and high light fluence increases the amount of heat produced. Thus, photodamage to viruses could occur if high light fluence is used. This study was also crucial in determining suitable light fluences to be used for subsequent photodynamic inactivation experiments. A suitable light fluence should not cause any significant damage and drastic reduction of virus titers. This was to rule out the photodamage effect and to ensure that any reduction in virus titers observed was due to the photodynamic action of the nanoparticles. In

this study, DENV2 suspension was exposed to NIR irradiation at different light doses and the extent of light photodamage was measured based on the virus titers determined by plaque assay.

Based on the results, NIR light photodamage to viruses increased with light fluence (Figure 5.4). The highest virus titer reduction was observed when DENV2 was irradiated at the fluence of 160 kJ/cm^2. At this fluence, DENV2 titer decreased by 2.12 $\log_{10}$ PFU/mL compared to the dark control for the same fluence. 1.3 $\log_{10}$ PFU/mL reduction was recorded when DENV2 was irradiated at the fluence of 80 kJ/cm^2 while less than 1 $\log_{10}$ PFU/mL reduction in virus titers were obtained for 20 and 40 kJ/cm^2. The reduction in virus titers compared to dark controls was statistically significant ($P < 0.05$) for DENV2 irradiated at fluences of 80 and 160 kJ/cm^2. Less than 5 % reduction was observed when fluence of 20 kJ/cm^2 was used to irradiate DENV2 while around 10 and 20 % reduction in virus titers were observed for 40 and 80 kJ/cm^2 (Figure 5.5). The highest percentage reduction of 32 % was observed for the fluence of 160 kJ/cm^2. Based on this study, light fluences up to 40 kJ/cm^2 could be used for subsequent photodynamic inactivation experiments as the the reduction in virus titers was statistically insignificant and the effect of photodamage to DENV2 was negligible (less than 1 $\log_{10}$ PFU/mL).

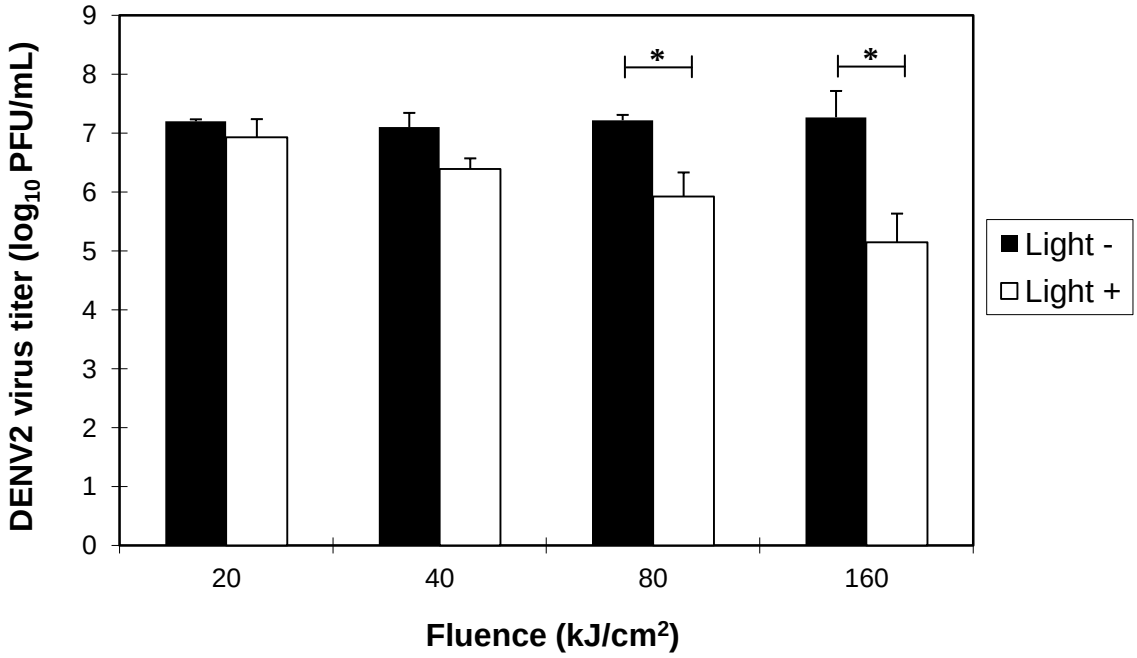

Figure 5.4 Infectious virus titers of DENV2 irradiated with different light fluences. All experiments were performed in triplicate and error bars represent standard deviations of the mean. Statistical analysis was done by comparing light-treated samples to their respective dark controls using Student's t-test, ***** $P < 0.05$.

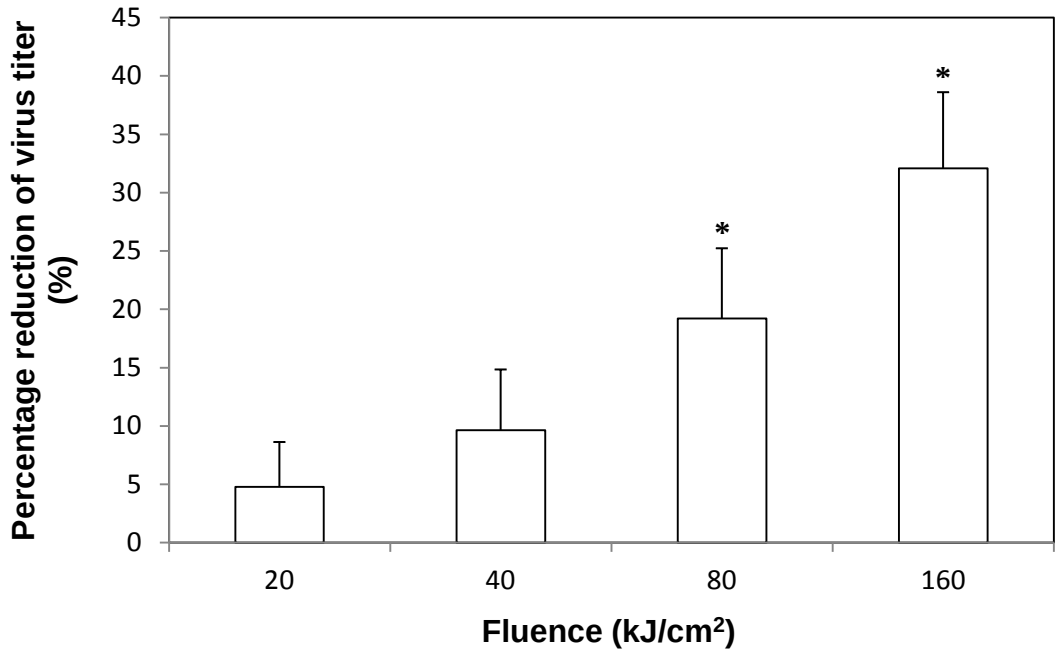

Figure 5.5 Percentage reduction of virus titer for DENV2 irradiated with different light fluences. Error bars represent standard deviations of the mean. Statistical analysis was done by comparing each of the DENV2 samples irradiated with 40, 80 and 160 kJ/cm^2 to the DENV2 sample irradiated with 20 kJ/cm^2, using Student's t-test, ***** $P < 0.05$.

5.3.3 Photodynamic inactivation of DENV2 in suspension with various concentrations of ZnPc-UCNs

We first examined the effect of nanoparticle concentrations on the photodynamic inactivation efficacy of this UCN-based system. Based on the previous light photodamage study, light fluence of 20 kJ/cm^2 caused negligible photodamage effect to viruses and was chosen as the light fluence for this study. DENV2 in L15 cell culture medium was mixed with various concentrations of ZnPc-MS-UCNs and irradiated at a fixed light dose of 20 kJ/cm^2. Another similar set of samples which acted as dark controls was prepared and kept in the dark without NIR irradiation. The results demonstrated that reduction in virus titers was concentration-dependent (Figure 5.6). Sample with the lowest nanoparticle concentration at 100 µg/mL was the least effective to photodynamically inactivate DENV2. At this concentration, the virus titer of the light-treated sample was 6.45 $\log_{10}$ PFU/mL, a 0.68 $\log_{10}$ PFU/mL or 9.6 % reduction (Figure 5.7) from its respective dark control sample. This reduction was just mildly lower than samples containing solely of DENV2 without any nanoparticle added (0 µg/mL). For this experimental set, the light-treated sample showed a reduction of 0.27 $\log_{10}$ PFU/mL when compared to its associated dark control sample. Significant virus titer reduction ($P < 0.05$) was seen for concentrations at 500 µg/mL and above. Virus titers reduced by more than half (52 % or 3.73 $\log_{10}$ PFU/mL reduction) when nanoparticle concentration of 500 µg/mL was used and further reduction of virus titer was recorded for nanoparticle concentration of 750 µg/mL which showed 5.66 $\log_{10}$ PFU/mL or 80 % reduction in virus titers compared to the same concentration in the dark. The best photodynamic inactivation efficacy was achieved when nanoparticles at the concentrations of 1000 µg/mL and onwards were used to intivate the viruses. Complete virus inactivation was observed for samples at 1000, 1250, 1500 and 2000 µg/mL of ZnPc-MS-UCNs, giving a 100 % reduction in virus titers. Meanwhile, for lower nanoparticle concentrations (100, 500, 750 and 1000 µg/mL), the virus

titers of their dark control samples remained stable and having around the same virus titer with the 0 μg/mL sample which only contained DENV2.

The virus titers of the dark control samples started to decrease when higher nanoparticle concentrations of 1250, 1500 and 2000 μg/mL were used. Compared to the DENV2 titer of 0 μg/mL at 7.12 $\log_{10}$ PFU/mL, these three concentrations of 1250, 1500 and 2000 μg/mL nanoparticles caused a much reduced titers at 5.58 $\log_{10}$ PFU/mL, 4.63 $\log_{10}$ PFU/mL and 2.45 $\log_{10}$ PFU/mL respectively. Compared to 0 μg/mL, 65 % reduction in virus titer, which was the sharpest decrease, was obtained when the highest nanoparticle concentration of 2000 μg/mL was used. The significant reduction in virus titers for dark control samples of higher nanoparticle concentrations was due to the toxicity of nanoparticles which echoed the same observation for the PEI-coated nanoparticles that caused complete virus inactivation at nanoparticle concentration of 2200 μg/mL. Although nanoparticle toxicity could also contribute to virus inactivation, it could possibly damage healthy cells or tissues if high amount of nanoparticles are to be used to treat localized tissue infections.

Overall, photodynamic inactivation efficacy increased with higher ZnPc-MS-UCN concentrations. High amount of nanoparticles was toxic to viruses. Taking the nanoparticle toxicity into account, ZnPc-UCN concentration of 1000 μg/mL produced the best photodynamic inactivation efficacy with no significant toxicity.

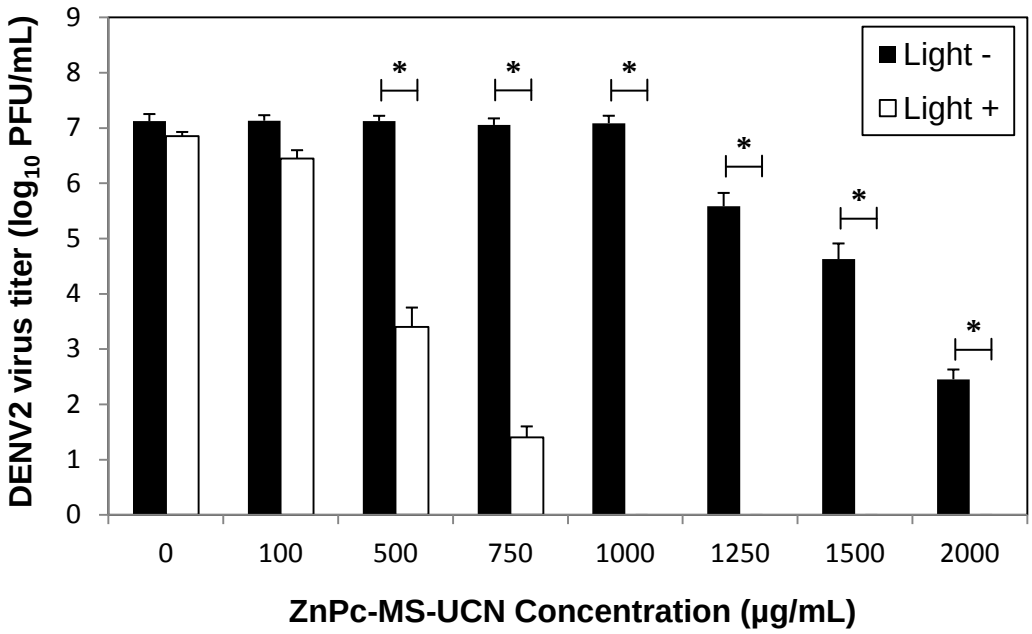

Figure 5.6 Infectious virus titers of DENV2 mixed with different ZnPc-MS-UCN concentrations and irradiated with 980 nm NIR light at the fluence of 20 kJ/cm^2. Nanoparticle toxicity was observed for ZnPc-MS-UCN concentrations of 1250 µg/mL and above. All experiments were performed in triplicate and error bars represent standard deviations of the mean. Statistical analysis was done by comparing light-treated samples to their respective dark controls using Student's t-test, ***** $P < 0.05$.

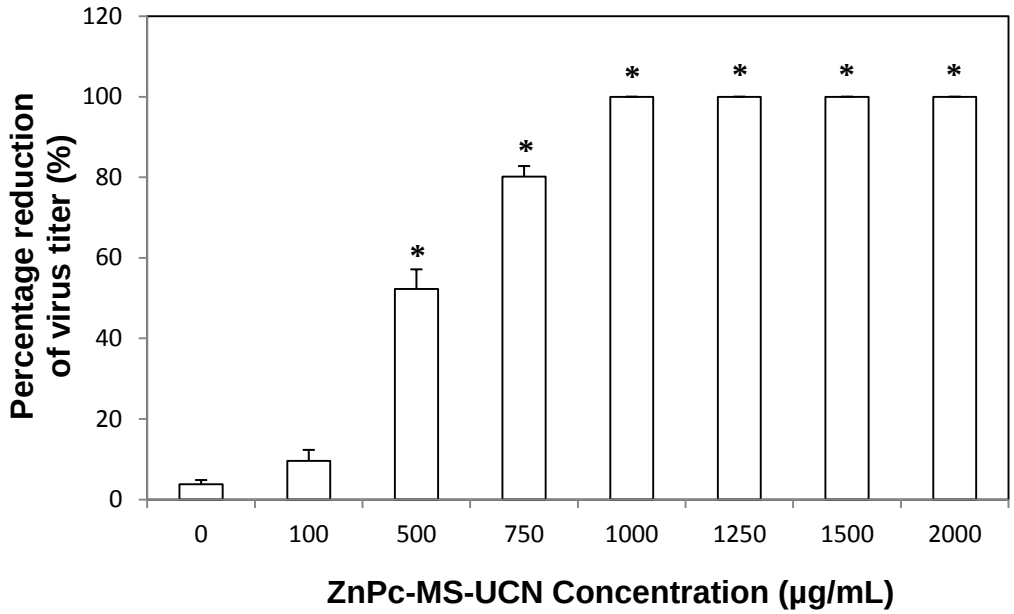

Figure 5.7 Percentage reduction of virus titer for DENV2 mixed with different concentrations of ZnPc-MS-UCN and irradiated with 980 nm NIR light at the fluence of 20 kJ/cm^2. Error bars represent standard deviations of the mean. Statistical analysis was done by comparing each of the samples to the control, 0 µg/mL (DENV2-only sample), using Student's t-test, ***** $P < 0.05$.

5.3.4 Photodynamic inactivation of DENV2 in suspension with different light fluences

Apart from concentration of nanoparticles, we further studied the effect of light fluence on the photodynamic inactivation efficacy of these nanoparticles. By fixing laser power, higher light fluence can be achieved by increasing the irradiation time, thus increasing the energy delivered to the irradiation site as well. Different light fluences were used in this study so as to explore the relationship between light fluence and photodynamic inactivation efficacy of the nanoparticles. Similar to the concentration of nanoparticles, the results demonstrated that photodynamic inactivation ability of ZnPc-MS-UCNs was light fluence-dependent. Virus titers of the light-treated samples reduced steadily from 3.44 $\log_{10}$ PFU/mL to 1.81 $\log_{10}$ PFU/mL upon NIR irradiation with light fluences ranging from 20 to 60 kJ/cm^2 (Figure 5.8). The percentage reduction of virus titers was further increased from 52 % at 20 kJ/cm^2 to 74 % at 60 kJ/cm^2, giving a 20 % more reduction in virus titers (Figure 5.9). By fixing the nanoparticle concentration at 500 μg/mL, photodynamic inactivation efficacy can be improved by delivering higher light fluence to the nanoparticles. Thus, effective photodynamic inactivation condition can be achieved by tuning the combination of nanoparticle concentrations and light doses while keeping the toxicity of nanoparticles and light photodamage to as minimum as possible.

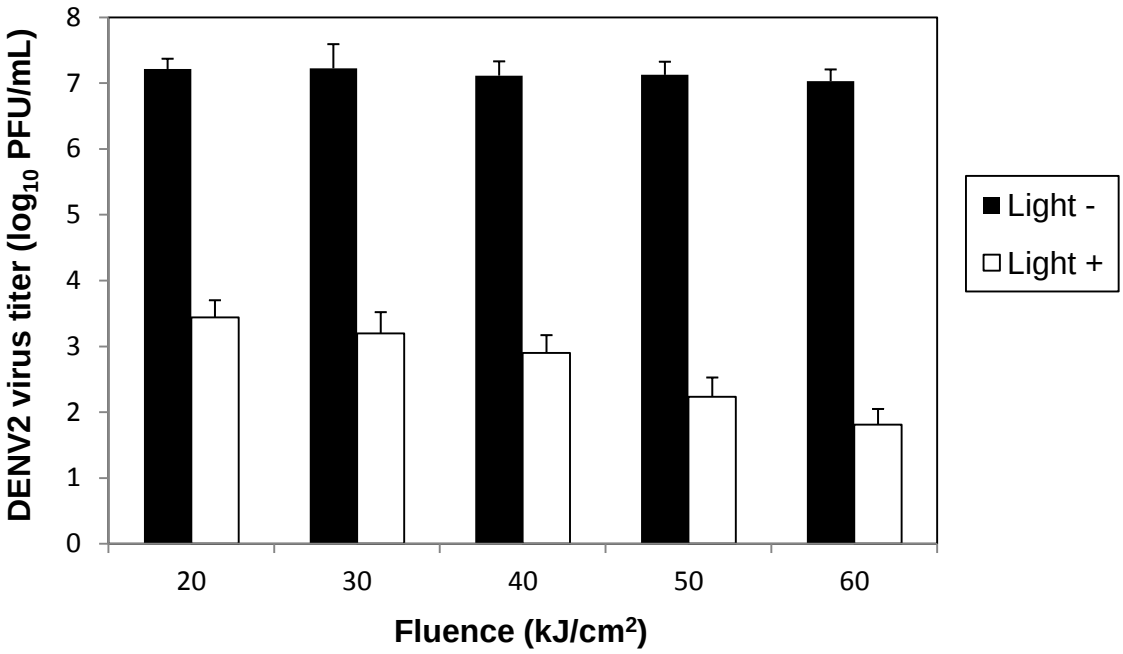

Figure 5.8 Infectious virus titers of DENV2 mixed with 0.5 mg/mL ZnPc-MS-UCNs and irradiated with 980 nm NIR light at different light fluences. All experiments were performed in triplicate and error bars represent standard deviations of the mean.

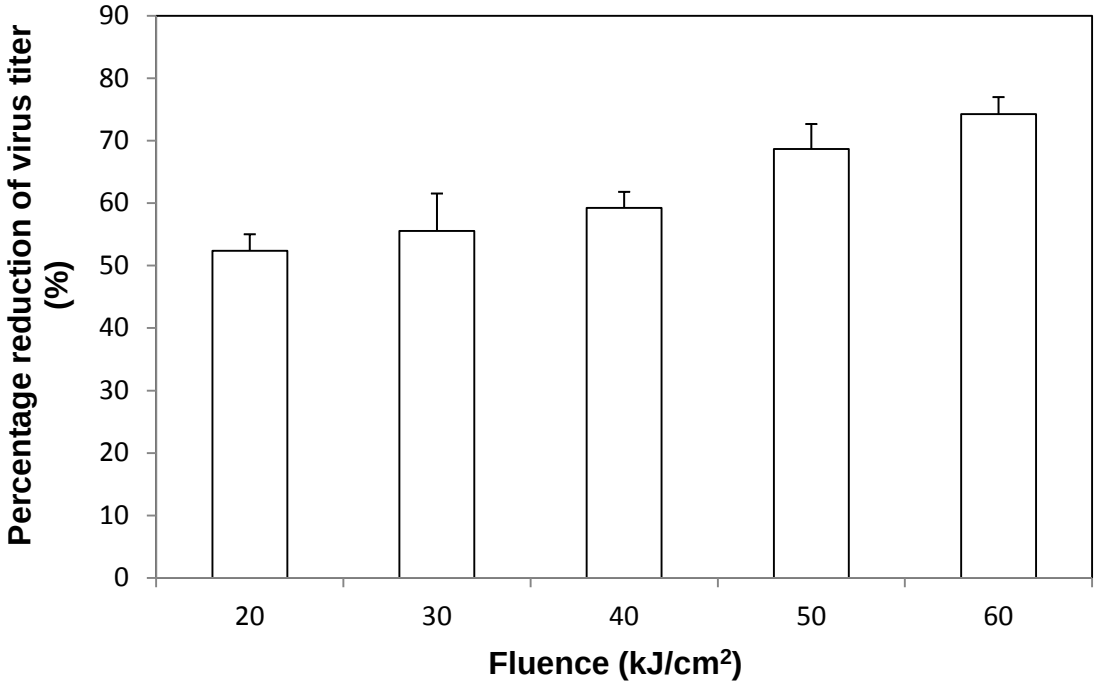

Figure 5.9 Percentage reduction of virus titer for DENV2 mixed with 0.5 mg/mL ZnPc-MS-UCNs and irradiated with 980 nm NIR light at different light fluences. Error bars represent standard deviations of the mean.

5.3.5 Photodynamic inactivation of viruses in a tissue model

5.3.5.1 NIR light attenuation of mouse tissue

Previous light attenuation study (as described in Section 5.3.1) had shown that NIR light was not attenuated by components of a typical sample used for photodynamic inactivation experiments. We further this light attenuation studies to investigate the tissue penetration depth of the NIR light. Mouse skin tissues of three different thicknesses were used for the study and the experimental design and procedures were described in Section 5.2.5. A control sample of DENV2 and ZnPc-MS-UCNs in L15 medium exposing to NIR irradiation without the mouse skin tissues was used for comparison. For all three tissue thicknesses, the NIR intensity reduced when the samples were irradiated with five different laser powers. (Figure 5.10). Light attenuation was not observed for the control sample. Higher intensity was observed when stronger laser power was used, suggesting that light-tissue penetration is laser power-dependent. This was to be expected as higher laser powers with more intense energy can penetrate deeper into the tissue than lower laser powers. Compared to the control sample, the percentage reduction of NIR intensity for sample with 1 mm tissue thickness was between 33 – 48 %, further increased to between 72 – 83 % for sample with 5mm tissue thickness and recorded a reduction of between 91 – 97 % for sample with 10 mm tissue thickness (Figure 5.11). Depending on the tissue thickness, the NIR light has shown the ability to penetrate mouse skin tissues. The NIR light can penetrate 1 and 5 mm thick tissues and even to the extent of 10 mm tissue depth albeit with much lower intensity. NIR light has been shown to have better tissue penetration ability than visible light. Visible light at 410 nm has been reported to penetrate only 1 to 2 mm into skin and increases up to 6 mm at 635 nm [74]. Studies to measure the penetration depth of various human tissues have shown that NIR light is able to penetrate deeper than red light for all measured tissues [75]. The observation that

the NIR intensity decreased with increasing tissue thickness could be attributed to the scattering and internal reflection properties of the tissues which could reduce the amount of light to be delivered to the target [76].

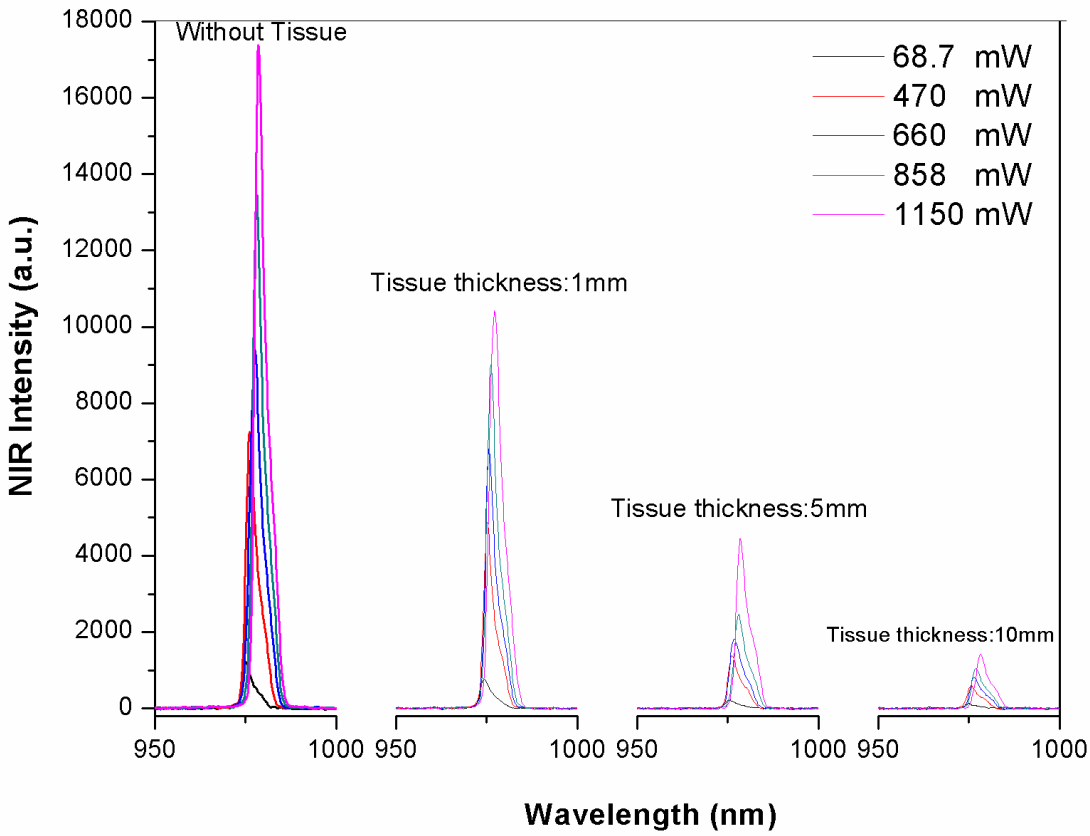

Figure 5.10 NIR intensities of samples (DENV2 and ZnPc-MS-UCNs in L15 medium) beneath mouse skin tissues of different thicknesses.

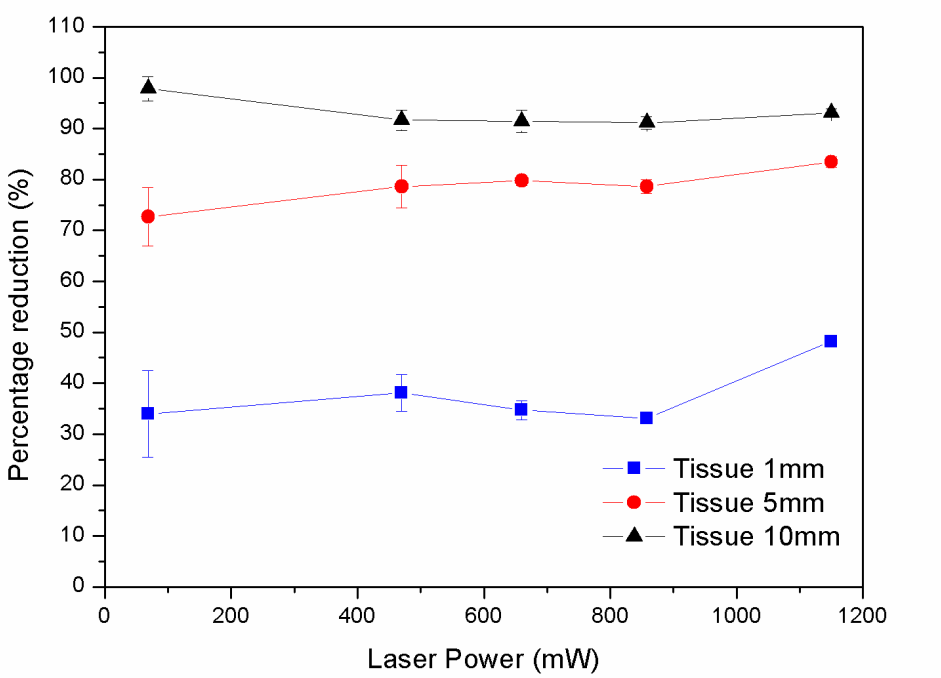

Figure 5.11 Percentage reduction of NIR intensity for samples beneath mouse tissues of different thicknesses. Error bars represent standard deviations of the mean. All experiments were performed in triplicate and error bars represent standard deviations of the mean.

5.3.5.2 Photodynamic inactivation of DENV2 beneath the mouse tissues

A preliminary study was performed to investigate the possibility of inactivating viruses photodynamically beneath the tissues. As tissues were involved in this study, a skin charring test was done to determine a suitable range of laser powers to be used in order to avoid burning, charring or any damage to the skin tissues due to high powers and long-term irradiation. In this test, female C57BL/6 mice was irradiated with 980 nm NIR light continuously for 1 h using laser powers in the range of 145 – 638 mW. At any one time, each mouse was irradiated with a fixed laser power for 1 h and the mice were observed for skin charring post laser treatment. After irradiation, laser power above 294 nm was shown to cause skin charring while laser power range of 145 – 294 mW did not show any skin charring (Table 5.3).

Laser power measured (mW)	Skin charring observed?
638	Yes
615	Yes
588	Yes
564	Yes
541	Yes
518	Yes
423	Yes
405	Yes
381	Yes
357	Yes
331	Slightly yes
294	No
195	No
145	No

Table 5.3 Post laser treatment skin charring observation of C57BL/6 mice irradiated for 1 h at different laser power. *(Courtesy of Ms. Niagara Muhammad Idris)*

Laser power of 284 mW (0.284 W), which falls in the range of 145 – 294 mW was used for the subsequent photodynamic inactivation study. Mouse skin tissues of 5 mm thick was used to cover wells which contained DENV2 in L15 medium added with ZnPc-MS-UCNs of different concentrations in a 96-well tissue culture plate. The experimental set-up and procedures were described in Section 5.2.8. Concentration-dependent reduction of virus titers was observed when the samples were being irradiated in the presence of 5 mm mouse skin

tissues (Figure 5.12). These results were consistent with the photodynamic inactivation of DENV2 in suspension (Section 5.3.3). However, the photodynamic inactivation efficacy in the presence of mouse skin tissues was generally lower in comparison with the efficacy of samples in suspension without tissues. Upon comparing with their respective dark control samples, less than 2 $\log_{10}$ PFU/mL reductions were observed for nanoparticle concentrations of 100, 500 and 750 μg/mL with percentage reduction of 14.7, 15.9 and 24.8 % respectively (Figure 5.13). Significant reduction in virus titers was only observed for nanoparticle concentration of 1000 μg/mL and above. A reduction range of 3.02 – 4.18 $\log_{10}$ PFU/mL (42 – 90 % reduction) from their associated dark control samples was obtained for ZnPc-MS-UCN concentrations of 1000, 1250 and 1500 μg/mL. Complete virus inactivation was achieved for sample with the highest nanoparticle concentration of 2000 μg/mL ZnPc-MS-UCNs, giving a 100 % reduction.

For ZnPc-UCN concentrations of 1250, 1500 and 2000 μg/mL, the virus titers of their dark control samples (Light -) showed that the nanoparticles were toxic to DENV2 at these concentrations. Compared to the virus titer of 0 μg/mL dark control sample which contained only DENV2 (7.12 $\log_{10}$ PFU/mL), the virus titers of these three concentrations decreased drastically to 5.48 $\log_{10}$ PFU/mL, 4.63 $\log_{10}$ PFU/mL and 2.32 $\log_{10}$ PFU/mL respectively.

This study has shown the ability of NIR light to penetrate mouse skin tissues at 5 mm and photodynamically inactivate DENV2 beneath the tissues. Nevertheless, with increasing nanoparticle concentrations, virus titers were reduced significantly. ZnPc-MS-UCN concentration of 1000 μg/mL gave the best photodynamic inactivation efficacy without causing any significant toxicity to the viruses.

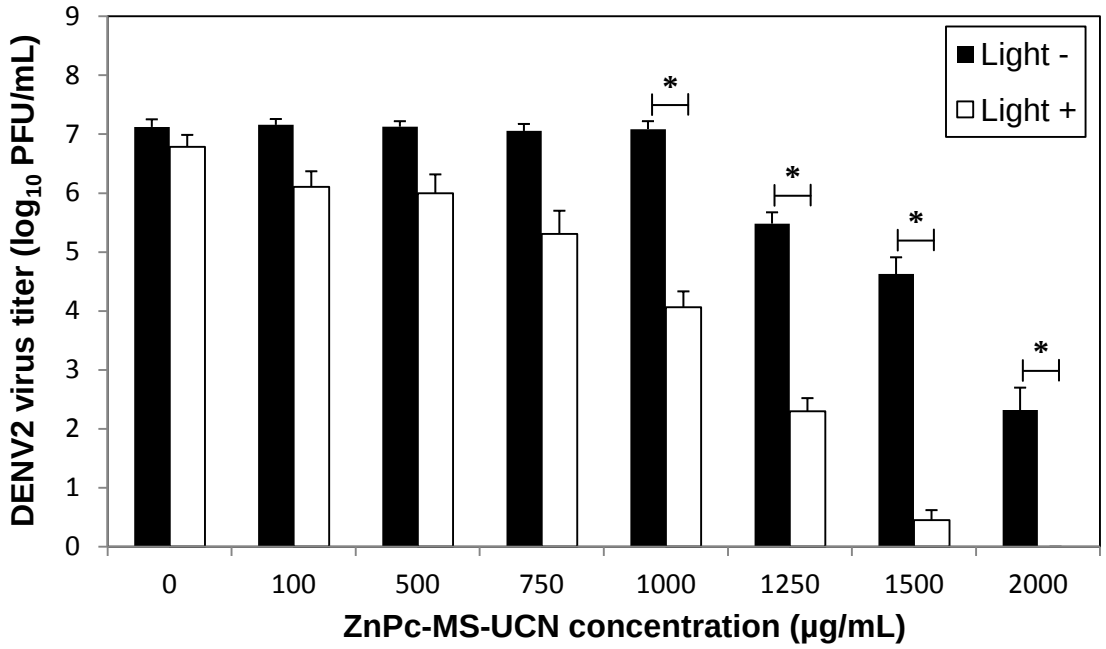

Figure 5.12 Infectious virus titers of DENV2 mixed with different ZnPc-MS-UCN concentrations beneath 5 mm thick mouse skin tissues and irradiated with 980 nm NIR light at the fluence of 40 kJ/cm^2. All experiments were performed in triplicate and error bars represent standard deviations of the mean. Statistical analysis was done by comparing light-treated samples to their respective dark controls using Student's t-test, ***** $P < 0.05$.

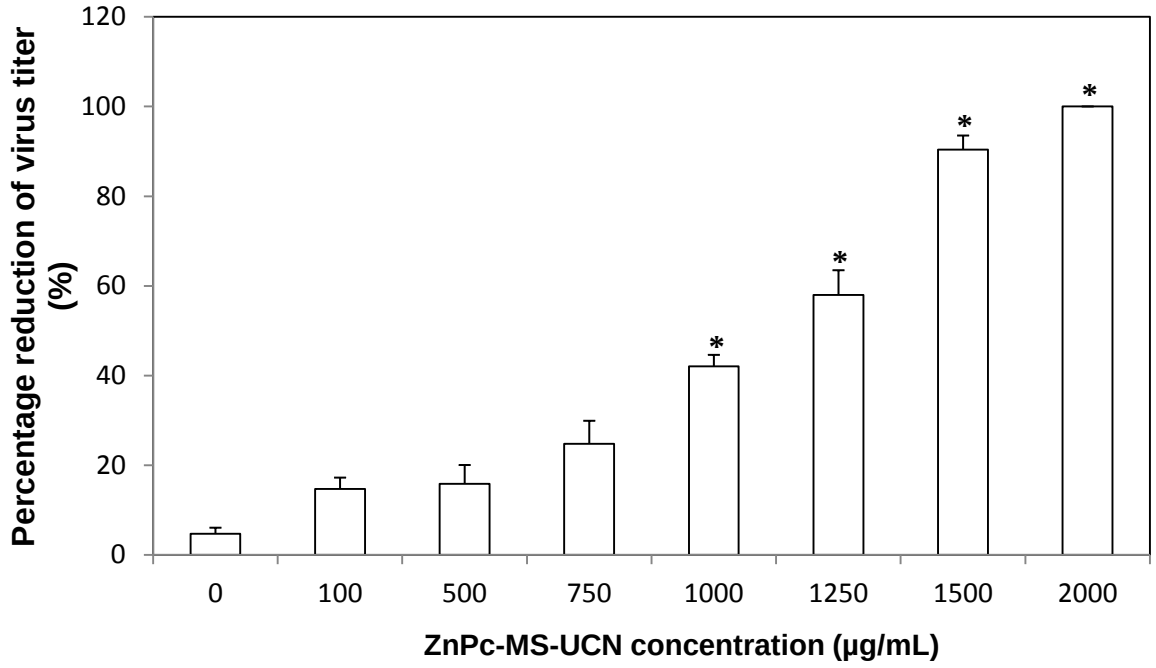

Figure 5.13 Percentage reduction of virus titers for DENV2 in different ZnPc-MS-UCN concentrations beneath 5 mm thick mouse skin tissues and irradiated at 980 nm NIR light at the fluence of 40 kJ/cm^2. Error bars represent standard deviations of the mean. Statistical analysis was done by comparing each of the samples to the control, 0 µg/mL (DENV2-only sample), using Student's t-test, ***** $P < 0.05$.

5.4 Conclusions

Upon NIR irradiation at 980 nm, the ZnPc-loaded mesoporous silica-coated nanoparticles photodynamically inactivated DENV2 in suspension in concentration- and light dose-dependent manners. NIR light at 980 nm was able to penetrate mouse skin tissues of 5 mm and inactivated the DENV2 in suspension beneath the tissues. Higher concentrations of nanoparticles were toxic to viruses, which may also toxic to cells and tissues. The combination of nanoparticle concentration and light fluence can be further optimized to achieve effective photodynamic inactivation with minimal or no toxicity caused to the healthy cells and tissues.

Chapter 6: Conclusions and future work

6.1 Main conclusions

We report here a novel antiviral approach to inactivate viruses via UCN-based photodynamic inactivation strategy. This is the first report of such inactivation strategy to be shown against viruses. The feasibility of this strategy was first displayed by the photodynamic inactivation of DENV2 in suspension by ZnPc-PEI-UCNs and was shown to be nanoparticle concentration-dependent.

The nanoparticle design of ZnPc-PEI-UCN was relooked and an improved version of UCNs in the form of mesoporous silica-coated UCNs were synthesized. These nanoparticles were characterized to possess porous silica structures to store photosensitizers. ZnPc photosensitizers were loaded into the pores of mesoporous silica using the ZnPc loading concentration showing the best singlet oxygen profile. The porous structures of silica allow the release of singlet oxygen from the nanoparticles to the surroundings with ease. Most importantly, the hydrophobic ZnPc photosensitizers remain strongly in the pores when incubated in aqueous solutions. Moreover, the porous silica protects photosensitizers from being degraded in the harsh biological environment.

Similar to the ZnPc-PEI-UCNs, the ZnPc-Si-UCNs photodynamically inactivated DENV2 in suspension in a concentration-dependent manner. In addition, the photodynamic inactivation was shown to be light dosage-dependent also. NIR light at 980 nm was shown to penetrate 5 mm thick mouse skin tissues and inactivated the DENV2 in suspension beneath the tissue. This signifies the advantages of using NIR-to-visible UCNs which get excited by NIR light that possesses high light penetration depth *in vivo* and emit visible radiations necessary to

excite the photosensitizers. In view of nanoparticle toxicity to viruses at higher concentrations, which may also toxic to cells and tissues, optimization of various parameters can be done to achieve effective photodynamic inactivation of viruses using optimum light dose and lower concentration of nanoparticles with minimal or no toxicity caused to the healthy cells and tissues.

6.2 Recommendations for future work

The feasibility of using UCNs for photodynamic inactivation of viruses has thus far been shown in cell culture suspension using Dengue virus as a model. Since this UCN-based system has been proven feasible to inactivate Dengue virus, the similar studies can be further applied to viruses causing localized infections such as herpesvirus and papillomavirus to provide a more realistic assessment of this system. In addition, this strategy can be further extended to study the photodynamic inactivation in virus-infected cellular system. As the cells have been infected by viruses, attempts should be made to remove intracellular viruses through direct killing of the infected cells as well as inactivate the extracellular viruses which are being released from cells into the cell culture medium. Internalization of ZnPc-loaded nanoparticles can first be done by incubating the nanoparticles with the infected cells before the cells were exposed to NIR irradiation. The PDT efficacy can then be evaluated by measuring cell viability and virus titer reduction via MTT assay and plaque assay respectively. MTT assay measures the percentage of surviving infected cells after PDT treatment while plaque assay measures infectious virus titer from the collected cell culture medium. The nanoparticles have been shown to be toxic to viruses at higher concentrations which raised concern about its toxicity to cells as well. To assess the nanoparticle toxicity, UCNs can be incubated in the dark with cells of interest at different nanoparticle

concentrations for a certain period of time and the cell viability can subsequnetly be measured via MTT assay.

On the other hand, a quantitative *in vivo* tissue penetration depth studies are needed to measure the extent of penetration distance and light energy that presents under the skin. The photodynamic inactivation of viruses beneath the tissues can be further studied by using different tissue thicknesses. To provide a more realistic assessment concerning the feasibility of UCN-based strategy in treating viruses beneath the tissues, a mouse model with localized virus infections should be created. The ZnPc-loaded nanoparticles at certain concentrations will then be injected directly to the localized infections site and the localized infected area will be exposed to NIR irradiation after a certain period of incubation time. Tissues will later be homogenized and virus titers determined via plaque assay.

Meanwhile, further investigation could also be performed to elucidate the underlying mechanism which causes the inactivation of viruses. Although Type II reaction which produces singlet oxygen is widely seen as the dominant reaction that mediates the photodynamic inactivation of viruses, the type I reaction which produces superoxides and hydroxyls may co-exist together with Type II reaction and contributes toward virus inactivation. The photodynamic inactivation effect on viral replication ability is also another important aspect to look into. Due to photodynamic damage, the viruses may either loss the ability to replicate in the host cells or incapable to recognize and bind to the host cells which significantly reduces the propagation and spread of viruses. In addition, the photodynamic inactivation damage to viral genome and envelope protein could also be examined. The knowledge that we gain from the photodynamic inactivation mechanism will greatly aid in the development of this UCN-based strategy for clinical use.

References

1. Brown SB, Brown EA, Walker I. The present and future role of photodynamic therapy in cancer treatment. *The Lancet Oncology* 5(8):497-508 (2004).
2. Huang Z. A review of progress in clinical photodynamic therapy. *Technology in Cancer Research and Treatment* 4(3):283 (2005).
3. Jori G, Fabris C, Soncin M, Ferro S, Coppellotti O, Dei D *et al.* Photodynamic therapy in the treatment of microbial infections: Basic principles and perspective applications. *Lasers in surgery and medicine* 38(5):468-481 (2006).
4. Raab O. Ueber die wirkung uoreszierenden stoffe auf infusorien. *Zeitung Biologie* 39:524-526 (1900).
5. Wainwright M. Photoinactivation of viruses. *Photochemical and Photobiological Sciences* 3(5):406-411 (2004).
6. Felber TD, Smith EB, Knox JM, Wallis C, Melnick JL. Photodynamic inactivation of herpes simplex: Report of a clinical trial. *Journal of the American Medical Association* 223(3):289-292 (1973).
7. Wainwright M. Local treatment of viral disease using photodynamic therapy. *International Journal of Antimicrobial Agents* 21(6):510-520 (2003).
8. De M, Ghosh PS, Rotello VM. Applications of nanoparticles in biology. *Advanced Materials* 20(22):4225-4241 (2008).
9. Dolmans DEJGJ, Fukumura D, Jain RK. Photodynamic therapy for cancer. *Nature Reviews Cancer* 3(5):380-387 (2003).
10. Henderson BW, Dougherty TJ. How does photodynamic therapy work? *Photochemistry and Photobiology* 55(1):145-157 (1992).
11. Foote CS. Definition of type I and type II photosensitized oxidation. *Photochemistry and Photobiology* 54(5):659-659 (1991).
12. Bechet D, Couleaud P, Frochot C, Viriot ML, Guillemin F, Barberi-Heyob M. Nanoparticles as vehicles for delivery of photodynamic therapy agents. *Trends in Biotechnology* 26(11):612-621 (2008).
13. Moan J, Berg K. The photodegradation of porphyrins in cells can be used to estimate the lifetime of singlet oxygen. *Photochemistry and Photobiology* 53(4):549-553 (1991).

14. Hatz S, Lambert JDC, Ogilby PR. Measuring the lifetime of singlet oxygen in a single cell: Addressing the issue of cell viability. *Photochemical and Photobiological Sciences* 6(10):1106-1116 (2007).
15. O'Riordan K, Akilov OE, Hasan T. The potential for photodynamic therapy in the treatment of localized infections. *Photodiagnosis and Photodynamic Therapy* 2(4):247-262 (2005).
16. Buytaert E, Dewaele M, Agostinis P. Molecular effectors of multiple cell death pathways initiated by photodynamic therapy. *Biochimica et Biophysica Acta (BBA)-Reviews on Cancer* 1776(1):86-107 (2007).
17. Chatterjee DK, Fong LS, Zhang Y. Nanoparticles in photodynamic therapy: An emerging paradigm. *Advanced Drug Delivery Reviews* 60(15):1627-1637 (2008).
18. Oleinick NL, Morris RL, Belichenko I. The role of apoptosis in response to photodynamic therapy: What, where, why, and how. *Photochemical and Photobiological Sciences* 1(1):1-21 (2002).
19. Bonnett R. Photosensitizers of the porphyrin and phthalocyanine series for photodynamic therapy. *Chemical Society Reviews* 24(1):19-33 (1995).
20. Von Tappeiner H, Jesionek A. Therapeutische versuche mit fluoreszierenden stoffen. *Muench Med Wochenschr* 47:2042-2044 (1903).
21. Dougherty TJ, Grindey G, Fiel R, Weishaupt KR, Boyle D. Photoradiation therapy. II. Cure of animal tumors with hematoporphyrin and light. *Journal of the National Cancer Institute* 55(1):115 (1975).
22. Dimofte A, Zhu TC, Hahn SM, Lustig RA. In vivo light dosimetry for motexafin lutetium mediated PDT of recurrent breast cancer. *Lasers in Surgery and Medicine* 31(5):305-312 (2002).
23. Hornung R. Photomedical approaches for the diagnosis and treatment of gynecologic cancers. *Current Drug Targets-Immune, Endocrine & Metabolic Disorders* 1(2):165-177 (2001).
24. Schweitzer V. Photodynamic therapy for treatment of head and neck cancer. *Otolaryngology-Head and Neck Surgery* 102(3):225 (1990).
25. Barr H, Krasner N, Boulos P, Chatlani P, Bown S. Photodynamic therapy for colorectal cancer: A quantitative pilot study. *British Journal of Surgery* 77(1):93-96 (1990).

26. Taber SW, Fingar VH, Coots CT, Wieman TJ. Photodynamic therapy using mono-L-aspartyl chlorin e6 (Npe6) for the treatment of cutaneous disease: A phase I clinical study. *Clinical Cancer Research* 4(11):2741 (1998).
27. Delaney TF, Sindelar WF, Tochner Z, Smith PD, Friauf WS, Thomas G *et al.* Phase I study of debulking surgery and photodynamic therapy for disseminated intraperitoneal tumors. *International Journal of Radiation Oncology* Biology* Physics* 25(3):445-457 (1993).
28. Bown S, Rogowska A, Whitelaw D, Lees W, Lovat L, Ripley P *et al.* Photodynamic therapy for cancer of the pancreas. *Gut* 50(4):549 (2002).
29. Schultz E. Inactivation of *staphyloccus* bacteriophage by methylene blue. *Experimental Biology and Medicine* 26(2):100 (1928).
30. Rapp F, Kemeny BA. Oncogenic potential of herpes simplex virus in mammalian cells following photodynamic inactivation. *Photochemistry and Photobiology* 25(4):335-337 (1977).
31. Berger RS, Papa CM. Photodye herpes therapy-cassandra confirmed? *Journal of the American Medical Association* 238(2):133 (1977).
32. Moore C, Wallis C, Melnick JL, Kuns MD. Photodynamic treatment of herpes keratitis. *Infection and Immunity* 5(2):169 (1972).
33. Lytle CD, Hester LD. Photodynamic treatment of herpes simplex virus infection in vitro. *Photochemistry and Photobiology* 24(5):443-448 (1976).
34. Goldenberg RL, Nelson K. Dermatitis from neutral red therapy of herpes genitalis. *Obstetrics & Gynecology* 46(3):359 (1975).
35. Yen GSL, Simon EH. Photosensitization of herpes simplex virus type 1 with neutral red. *Journal of General Virology* 41(2):273 (1978).
36. Speck WT, Santella RM, Brem S, Rosenkranz HS. Alteration of human cellular DNA by neutral red in the presence of visible light. *Mutation Research* 66(1):95 (1979).
37. Lytle C, Carney P, Felten R, Bushar H, Straight R. Inactivation and mutagenesis of herpes virus by photodynamic treatment with therapeutic dyes. *Photochemistry and Photobiology* 50(3):367-371 (1989).
38. Abramson AL, Hirschfield LS, Shikowitz MJ, Barrezueta NX. The pathologic effects of photodynamic therapy on the larynx: Experimental study. *Archives of Otolaryngology-Head and Neck Surgery* 114(1):33 (1988).

39. Mullooly VM, Abramson AL, Shikowitz MJ. Dihematoporphyrin ether induced photosensitivity in laryngeal papilloma patients. *Lasers in Surgery and Medicine* 10(4):349-356 (1990).
40. Bauman NM, Smith RJH. Recurrent respiratory papillomatosis. *Pediatric Clinics of North America* 43(6):1385-1401 (1996).
41. Gilbert DJ. Incorporating photodynamic therapy into a medical and cosmetic dermatology practice. *Dermatologic Clinics* 25(1)(2007).
42. Smetana Z, Malik Z, Orenstein A, Mendelson E, Ben Hur E. Treatment of viral infections with 5 aminolevulinic acid and light. *Lasers in Surgery and Medicine* 21(4):351-358 (1997).
43. Gold MH, Moiin A. Treatment of verrucae vulgaris and molluscum contagiosum with photodynamic therapy. *Dermatologic Clinics* 25(1)(2007).
44. Wainwright M. Methylene blue derivatives-suitable photoantimicrobials for blood product disinfection? *International Journal of Antimicrobial Agents* 16(4):381-394 (2000).
45. Lambrecht B, Mohr H, Knuever-Hopf J, Schmitt H. Photoinactivation of viruses in human fresh plasma by phenothiazine dyes in combination with visible light. *Vox Sanguinis* 60(4):207-213 (1991).
46. Snyder E, McCullough J, Slichter SJ, Strauss RG, Lopez Plaza I, Lin JS *et al.* Clinical safety of platelets photochemically treated with amotosalen HCl and ultraviolet A light for pathogen inactivation: The SPRINT trial. *Transfusion* 45(12):1864-1875 (2005).
47. Ruane PH, Edrich R, Gampp D, Keil SD, Leonard RL, Goodrich RP. Photochemical inactivation of selected viruses and bacteria in platelet concentrates using riboflavin and light. *Transfusion* 44(6):877-885 (2004).
48. Williamson LM, Cardigan R, Prowse CV. Methylene blue treated fresh frozen plasma: What is its contribution to blood safety? *Transfusion* 43(9):1322-1329 (2003).
49. Pohler P, Walker WH, Reichenberg S, Mohr H, Gravemann U, Muller TH. Methylene blue treated plasma: Pharmacokinetic and toxicological profile of MB and photoproducts. *Vox Sanguinis* 87(Suppl 3):119 (2004).
50. Soncin M, Polo L, Reddi E, Jori G, Kenney ME, Cheng G *et al.* Effect of the delivery system on the biodistribution of Ge (IV) octabutoxy-phthalocyanines in tumour-bearing mice. *Cancer Letters* 89(1):101-106 (1995).

51. Auzel F. Upconversion and anti-stokes processes with f and d ions in solids. *Chemical Reviews* 104(1):139-173 (2004).
52. Wang F, Liu X. Recent advances in the chemistry of lanthanide-doped upconversion nanocrystals. *Chemical Society Reviews* 38(4):976-989 (2009).
53. Kramer KW, Biner D, Frei G, Gudel HU, Hehlen MP, Luthi SR. Hexagonal sodium yttrium fluoride based green and blue emitting upconversion phosphors. *Chemistry of Materials* 16(7):1244-1251 (2004).
54. Chatterjee DK, Abdul Jalil R, Zhang Y. Upconversion fluorescence imaging of cells and small animals using lanthanide doped nanocrystals. *Biomaterials* 29(7):937-943 (2008).
55. Chatterjee DK, Yong Z. Upconverting nanoparticles as nanotransducers for photodynamic therapy in cancer cells. *Nanomedicine* 3(1):73-82 (2008).
56. Ungun B, Prud'homme RK, Budijono SJ, Shan J, Lim SF, Ju Y *et al.* Nanofabricated upconversion nanoparticles for photodynamic therapy. *Optics Express* 17(1):80-86 (2009).
57. Zhang P, Steelant W, Kumar M, Scholfield M. Versatile photosensitizers for photodynamic therapy at infrared excitation. *Journal of the American Chemical Society* 129(15):4526-4527 (2007).
58. Qian HS, Guo HC, Ho PCL, Mahendran R, Zhang Y. Mesoporous-silica-coated up-conversion fluorescent nanoparticles for photodynamic therapy. *Small* 5(20):2285-2290 (2009).
59. Guo H, Qian H, Idris NM, Zhang Y. Singlet oxygen-induced apoptosis of cancer cells using upconversion fluorescent nanoparticles as a carrier of photosensitizer. *Nanomedicine: Nanotechnology, Biology, and Medicine* 6(3):486-495 (2010).
60. Wang F, Chatterjee DK, Li Z, Zhang Y, Fan X, Wang M. Synthesis of polyethylenimine/$NaYF_4$ nanoparticles with upconversion fluorescence. *Nanotechnology* 17(23):5786-5791 (2006).
61. Calzavara Pinton P, Venturini M, Sala R. Photodynamic therapy: Update 2006 part 1: Photochemistry and photobiology. *Journal of the European Academy of Dermatology and Venereology* 21(3):293-302 (2007).
62. Konan YN, Gurny R, Allemann E. State of the art in the delivery of photosensitizers for photodynamic therapy. *Journal of Photochemistry and Photobiology B: Biology* 66(2):89-106 (2002).

63. Hunter AC. Molecular hurdles in polyfectin design and mechanistic background to polycation induced cytotoxicity. *Advanced Drug Delivery Reviews* 58(14):1523-1531 (2006).
64. Moghimi SM, Symonds P, Murray JC, Hunter AC, Debska G, Szewczyk A. A two-stage poly (ethylenimine)-mediated cytotoxicity: Implications for gene transfer/therapy. *Molecular Therapy* 11(6):990-995 (2005).
65. Munoz B, Ramila A, Perez-Pariente J, Diaz I, Vallet-Regi M. MCM-41 organic modification as drug delivery rate regulator. *Chemistry of Materials* 15(2):500-503 (2003).
66. Han YJ, Stucky GD, Butler A. Mesoporous silicate sequestration and release of proteins. *Journal of the American Chemical Society* 121(42):9897-9898 (1999).
67. Nann T, Mulvaney P. Single quantum dots in spherical silica particles. *Angewandte Chemie International Edition* 43(40):5393-5396 (2004).
68. Yi DK, Selvan ST, Lee SS, Papaefthymiou GC, Kundaliya D, Ying JY. Silica-coated nanocomposites of magnetic nanoparticles and quantum dots. *Journal of the American Chemical Society* 127(14):4990-4991 (2005).
69. Yoon TJ, Yu KN, Kim E, Kim JS, Kim BG, Yun SH *et al.* Specific targeting, cell sorting, and bioimaging with smart magnetic silica core-shell nanomaterials. *Small* 2(2):209-215 (2006).
70. Ricci-Junior E, Marchetti JM. Zinc (II) phthalocyanine loaded PLGA nanoparticles for photodynamic therapy use. *International Journal of Pharmaceutics* 310(1-2):187-195 (2006).
71. McCarthy JR, Perez JM, Bruckner C, Weissleder R. Polymeric nanoparticle preparation that eradicates tumors. *Nano Letters* 5(12):2552-2556 (2005).
72. Rijcken CJF, Hofman JW, van Zeeland F, Hennink WE, van Nostrum CF. Photosensitiser-loaded biodegradable polymeric micelles: Preparation, characterisation and in vitro pdt efficacy. *Journal of Controlled Release* 124(3):144-153 (2007).
73. Van Leengoed H, Cuomo V, Versteeg A, Van der Veen N, Jori G, Star W. In vivo fluorescence and photodynamic activity of zinc phthalocyanine administered in liposomes. *British Journal of Cancer* 69(5):840 (1994).
74. Morton CA. Photodynamic therapy for nonmelanoma skin cancer--and more? *Archives of Dermatology* 140(1):116 (2004).

75. Stolik S, Delgado J, Perez A, Anasagasti L. Measurement of the penetration depths of red and near infrared light in human. *Journal of Photochemistry and Photobiology B: Biology* 57(2-3):90-93 (2000).
76. Star WM. Light delivery and light dosimetry for photodynamic therapy. *Lasers in Medical Science* 5(2):107-113 (1990).